Deep inelastic cross-section measurements at large y with the ZEUS detector at HERA

H. Abramowicz,[27,p] I. Abt,[21] L. Adamczyk,[8] M. Adamus,[34] R. Aggarwal,[4] S. Antonelli,[2] O. Arslan,[3] V. Aushev,[16,17] Y. Aushev,[17,k] O. Bachynska,[10] A. N. Barakbaev,[15] N. Bartosik,[10] O. Behnke,[10] J. Behr,[10] U. Behrens,[10] A. Bertolin,[23] S. Bhadra,[36] I. Bloch,[11] V. Bokhonov,[16] E. G. Boos,[15] K. Borras,[10] I. Brock,[3] R. Brugnera,[24] A. Bruni,[1] B. Brzozowska,[33] P. J. Bussey,[12] A. Caldwell,[21] M. Capua,[5] C. D. Catterall,[36] J. Chwastowski,[7,b] J. Ciborowski,[33,r] R. Ciesielski,[10,c] A. M. Cooper-Sarkar,[22] M. Corradi,[1] F. Corriveau,[18] G. D'Agostini,[26] R. K. Dementiev,[20] R. C. E. Devenish,[22] G. Dolinska,[10] V. Drugakov,[11] S. Dusini,[23] J. Ferrando,[12] J. Figiel,[7] B. Foster,[13,h] G. Gach,[8] A. Garfagnini,[24] A. Geiser,[10] A. Gizhko,[10] L. K. Gladilin,[20] O. Gogota,[17] Yu. A. Golubkov,[20] J. Grebenyuk,[10] I. Gregor,[10] G. Grzelak,[33] O. Gueta,[27] M. Guzik,[8] W. Hain,[10] G. Hartner,[36] D. Hochman,[35] R. Hori,[14] Z. A. Ibrahim,[6] Y. Iga,[25] M. Ishitsuka,[28] A. Iudin,[17,k] F. Januschek,[10] I. Kadenko,[17] S. Kananov,[27] T. Kanno,[28] U. Karshon,[35] M. Kaur,[4] P. Kaur,[4] L. A. Khein,[20] D. Kisielewska,[8] R. Klanner,[13] U. Klein,[10,d] N. Kondrashova,[17,l] O. Kononenko,[17] Ie. Korol,[10] I. A. Korzhavina,[20] A. Kotański,[9] U. Kötz,[10] N. Kovalchuk,[17,m] H. Kowalski,[10] O. Kuprash,[10] M. Kuze,[28] B. B. Levchenko,[20] A. Levy,[27] V. Libov,[10] S. Limentani,[24] M. Lisovyi,[10] E. Lobodzinska,[10] W. Lohmann,[11] B. Löhr,[10] E. Lohrmann,[13] A. Longhin,[23,o] D. Lontkovskyi,[10] O. Yu. Lukina,[20] J. Maeda,[28,q] I. Makarenko,[10] J. Malka,[10] J. F. Martin,[31] S. Mergelmeyer,[3] F. Mohamad Idris,[6,a] K. Mujkic,[10,e] V. Myronenko,[10] K. Nagano,[14] A. Nigro,[26] T. Nobe,[28] D. Notz,[10] R. J. Nowak,[33] K. Olkiewicz,[7] Yu. Onishchuk,[17] E. Paul,[3] W. Perlański,[33,s] H. Perrey,[10] N. S. Pokrovskiy,[15] A. S. Proskuryakov,[20,*] M. Przybycień,[8] A. Raval,[10] P. Roloff,[10,f] I. Rubinsky,[10] M. Ruspa,[30] V. Samojlov,[15] D. H. Saxon,[12] M. Schioppa,[5] W. B. Schmidke,[21,n] U. Schneekloth,[10] T. Schörner-Sadenius,[10] J. Schwartz,[18] L. M. Shcheglova,[20] R. Shevchenko,[17,k] O. Shkola,[17,m] I. Singh,[4] I. O. Skillicorn,[12] W. Słomiński,[9] V. Sola,[13] A. Solano,[29] A. Spiridonov,[10,g] L. Stanco,[23] N. Stefaniuk,[10] A. Stern,[27] T. P. Stewart,[31] P. Stopa,[7] J. Sztuk-Dambietz,[13] D. Szuba,[13] J. Szuba,[10] E. Tassi,[5] T. Temiraliev,[15] K. Tokushuku,[14,i] J. Tomaszewska,[33,t] A. Trofymov,[17,m] V. Trusov,[17] T. Tsurugai,[19] M. Turcato,[13] O. Turkot,[10] T. Tymieniecka,[34] A. Verbytskyi,[21] O. Viazlo,[17] R. Walczak,[22] W. A. T. Wan Abdullah,[6] K. Wichmann,[10] M. Wing,[32] G. Wolf,[10] S. Yamada,[14] Y. Yamazaki,[14,j] N. Zakharchuk,[17,m] A. F. Żarnecki,[33] L. Zawiejski,[7] O. Zenaiev,[10] B. O. Zhautykov,[15] N. Zhmak,[16] and D. S. Zotkin[20]

(ZEUS Collaboration)

[1]*INFN Bologna, Bologna, Italy*
[2]*University and INFN Bologna, Bologna, Italy*
[3]*Physikalisches Institut der Universität Bonn, Bonn, Germany*
[4]*Department of Physics, Panjab University, Chandigarh, India*
[5]*Calabria University, Physics Department and INFN, Cosenza, Italy*
[6]*National Centre for Particle Physics, Universiti Malaya, 50603 Kuala Lumpur, Malaysia*
[7]*The Henryk Niewodniczanski Institute of Nuclear Physics, Polish Academy of Sciences, Krakow, Poland*
[8]*AGH-University of Science and Technology, Faculty of Physics and Applied Computer Science, Krakow, Poland*
[9]*Department of Physics, Jagellonian University, Cracow, Poland*
[10]*Deutsches Elektronen-Synchrotron DESY, Hamburg, Germany*
[11]*Deutsches Elektronen-Synchrotron DESY, Zeuthen, Germany*
[12]*School of Physics and Astronomy, University of Glasgow, Glasgow, United Kingdom*
[13]*Hamburg University, Institute of Experimental Physics, Hamburg, Germany*
[14]*Institute of Particle and Nuclear Studies, KEK, Tsukuba, Japan*
[15]*Institute of Physics and Technology of Ministry of Education and Science of Kazakhstan, Almaty, Kazakhstan*
[16]*Institute for Nuclear Research, National Academy of Sciences, Kyiv, Ukraine*
[17]*Department of Nuclear Physics, National Taras Shevchenko University of Kyiv, Kyiv, Ukraine*
[18]*Department of Physics, McGill University, Montréal, Quebec, Canada H3A 2T8*
[19]*Meiji Gakuin University, Faculty of General Education, Yokohama, Japan*
[20]*Lomonosov Moscow State University, Skobeltsyn Institute of Nuclear Physics, Moscow, Russia*
[21]*Max-Planck-Institut für Physik, München, Germany*
[22]*Department of Physics, University of Oxford, Oxford, United Kingdom*
[23]*INFN Padova, Padova, Italy*
[24]*Dipartimento di Fisica dell' Università and INFN, Padova, Italy*
[25]*Polytechnic University, Tokyo, Japan*
[26]*Dipartimento di Fisica, Università "La Sapienza" and INFN, Rome, Italy*

[27]*Raymond and Beverly Sackler Faculty of Exact Sciences, School of Physics, Tel Aviv University, Tel Aviv, Israel*
[28]*Department of Physics, Tokyo Institute of Technology, Tokyo, Japan*
[29]*Università di Torino and INFN, Torino, Italy*
[30]*Università del Piemonte Orientale, Novara, and INFN, Torino, Italy*
[31]*Department of Physics, University of Toronto, Toronto, Ontario, Canada M5S 1A7*
[32]*Physics and Astronomy Department, University College London, London, United Kingdom*
[33]*Faculty of Physics, University of Warsaw, Warsaw, Poland*
[34]*National Centre for Nuclear Research, Warsaw, Poland*
[35]*Department of Particle Physics and Astrophysics, Weizmann Institute, Rehovot, Israel*
[36]*Department of Physics, York University, Ontario, Canada M3J 1P3*
(Received 26 June 2014; published 7 October 2014)

The reduced cross sections for e^+p deep inelastic scattering have been measured with the ZEUS detector at HERA at three different center-of-mass energies, 318, 251 and 225 GeV. The cross sections, measured double differentially in Bjorken x and the virtuality, Q^2, were obtained in the region $0.13 \le y \le 0.75$, where y denotes the inelasticity and $5 \le Q^2 \le 110$ GeV^2. The proton structure functions F_2 and F_L were extracted from the measured cross sections.

DOI: 10.1103/PhysRevD.90.072002 PACS numbers: 12.38.-t, 12.38.Aw, 14.20.Dh

I. INTRODUCTION

Deep inelastic scattering (DIS) in $e^{\pm}p$ collisions is an important tool to investigate the structure of the proton and to test different theoretical approaches to solving quantum chromodynamics (QCD). At low virtuality, Q^2, the inclusive $e^{\pm}p$ DIS cross section can be expressed in terms of the two structure functions, F_2 and F_L, as

$$\frac{d^2\sigma^{e^{\pm}p}}{dxdQ^2} = \frac{2\pi\alpha^2 Y_+}{xQ^4}\left[F_2(x,Q^2) - \frac{y^2}{Y_+}F_L(x,Q^2)\right] = \frac{2\pi\alpha^2 Y_+}{xQ^4}\tilde{\sigma}(x,Q^2,y), \quad (1)$$

where α is the fine structure constant, x is the Bjorken scaling variable, y is the inelasticity and $Y_+ = 1+(1-y)^2$. The quantity $\tilde{\sigma}$ is referred to as the reduced cross section. The kinematic variables are related via $Q^2 = xys$, where $\sqrt{s}$ is the ep center-of-mass energy.

The magnitude of F_L is proportional to the absorption cross section for longitudinally polarized virtual photons by protons, $F_L \propto \sigma_L$, while F_2 includes also the absorption cross section for transversely polarized virtual photons, $F_2 \propto (\sigma_T + \sigma_L)$. At low values of x, the ratio $R = F_L/(F_2 - F_L) \approx \sigma_L/\sigma_T$ gives the relative strengths of the two components.

HERA measurements [1] of $\tilde{\sigma}$ provide the strongest constraints on the proton parton distribution functions (PDFs) at low x. Within the DGLAP formalism [2], F_2 at low x is dominated by the quark sea distributions while the scaling violations of F_2 reflect the gluon distribution.

The value of F_L is zero in zeroth-order perturbative QCD. Contributions to F_L arise from higher-order processes initiated by quarks and gluons in the proton. At low Q^2 and x, the gluon-initiated processes dominate and F_L is directly correlated to the gluon density. The description of the F_L contribution is the theoretically most challenging part in the QCD analysis (PDF extraction) of the HERA reduced cross-section data. The various available model calculations [3–9] differ sizably in their predictions of F_L, in particular at low Q^2.

This paper presents new measurements of the reduced e^+p cross sections up to large values of y using the ZEUS

[*]Deceased.
[a]Also at Agensi Nuklear Malaysia, 43000 Kajang, Bangi, Malaysia.
[b]Also at Cracow University of Technology, Faculty of Physics, Mathematics and Applied Computer Science, Poland.
[c]Present address: Rockefeller University, New York, NY 10065, USA.
[d]Present address: University of Liverpool, United Kingdom.
[e]Also affiliated with University College London, United Kingdom.
[f]Present address: CERN, Geneva, Switzerland.
[g]Also at Institute of Theoretical and Experimental Physics, Moscow, Russia.
[h]Alexander von Humboldt Professor; also at DESY and University of Oxford.
[i]Also at University of Tokyo, Japan.
[j]Present address: Kobe University, Japan.
[k]Member of National Technical University of Ukraine, Kyiv Polytechnic Institute, Kyiv, Ukraine.
[l]Present address: DESY ATLAS group.
[m]Member of National University of Kyiv–Mohyla Academy, Kyiv, Ukraine.
[n]Present address: BNL, USA.
[o]Present address: LNF, Frascati, Italy.
[p]Also at Max Planck Institute for Physics, Munich, Germany, External Scientific Member.
[q]Present address: Tokyo Metropolitan University, Japan.
[r]Also at Łódź University, Poland.
[s]Member of Łódź University, Poland.
[t]Present address: Polish Air Force Academy in Deblin.

detector. The data were taken at different center-of-mass energies, $\sqrt{s} = 318$, 251, and 225 GeV, allowing for measurements at fixed (x, Q^2) but different values of y. This allows F_2 to be decoupled from F_L, thus providing direct sensitivity to the gluon density. The variation of $\sqrt{s}$ was achieved by varying the proton beam energy, E_p, while keeping the electron[1] beam energy constant, $E_e = 27.5$ GeV. The data were collected in 2006 and 2007 with $E_p = 920$, 575, and 460 GeV, referred to respectively as the high-(HER), medium-(MER) and low-energy-running (LER) samples. The corresponding integrated luminosities of the HER, MER and LER samples are 44.5, 7.1, and 13.9 pb^{-1}, respectively. The cross-section measurements at fixed (x, Q^2) and different y were used to extract F_2 and F_L separately, as has been previously done in fixed-target experiments [10–13], and recently by the ZEUS [14] and H1 [15–18] collaborations at HERA. For the results reported in this paper, high-precision data taken with an 820 GeV proton beam [19] were also included in the extraction. This data set, referred to as the ZEUS97 sample, has an integrated luminosity of 30.0 pb^{-1}.

The data described here supersede those in the previous publication [14]. The main improvements with respect to the previous analysis are an extension of the kinematic coverage of the measurements to lower values of Q^2, improved analysis techniques and a better understanding of systematic uncertainties, leading to more accurate and more precise measurements of the reduced cross sections.

II. THE ZEUS DETECTOR

A detailed description of the ZEUS detector can be found elsewhere [20]. A brief outline of the components most relevant for this analysis is given below.

In the kinematic range of the analysis, charged particles were tracked in the central tracking detector (CTD) [21] and the microvertex detector (MVD) [22]. These components operated in a magnetic field of 1.43 T provided by a thin superconducting solenoid. The CTD drift chamber covered the polar-angle region[2] $15° < \theta < 164°$. The MVD silicon tracker consisted of a barrel (BMVD) and a forward (FMVD) section. The BMVD provided polar-angle coverage for tracks from 30° to 150°. The FMVD extended the polar-angle coverage in the forward region to 7°. For CTD-MVD tracks that pass through all nine CTD superlayers, the momentum resolution was $\sigma(p_T)/p_T = 0.0029 p_T \oplus 0.0081 \oplus 0.0012/p_T$, with p_T in GeV.

The high resolution uranium-scintillator calorimeter (CAL) [23] consisted of three parts: the forward (FCAL), the barrel (BCAL) and the rear (RCAL) calorimeters. Each part was subdivided transversely into towers and longitudinally into one electromagnetic section and either one (in RCAL) or two (in BCAL and FCAL) hadronic sections. The smallest subdivision of the calorimeter was called a cell. The CAL energy resolutions, as measured under test-beam conditions, were $\sigma(E)/E = 0.18/\sqrt{E}$ for electrons and $\sigma(E)/E = 0.35/\sqrt{E}$ for hadrons, with E in GeV.

The rear hadron-electron separator (RHES) [24] consisted of a layer of approximately 10 000 (3×3 cm^2) silicon-pad detectors inserted in the RCAL at a depth of approximately three radiation lengths. The small-angle rear tracking detector (SRTD) [25] was attached to the front face of the RCAL and consisted of two planes of scintillator strips. The detector covers the total area of 68×68 cm^2, with a 20×20 cm^2 cutout in the center for the beam pipe. The polar-angle coverage is $162° < \theta < 176°$, with full acceptance for $167° < \theta < 174.5°$.

A small tungsten-scintillator calorimeter located approximately 6 m from the interaction point in the rear direction is referred to as the 6 m-Tagger [26]. For scattered electrons at small scattering angles in the energy range from 4.1 to 7.4 GeV, the acceptance was very close to unity with very high purity.

The luminosity was measured using the Bethe-Heitler reaction $ep \to e\gamma p$ by a luminosity detector which consisted of independent lead-scintillator calorimeter [27] and magnetic spectrometer [28] systems. The fractional systematic uncertainty on the measured luminosity was 1.8% [29], composed of a correlated uncertainty of 1.5% for the HER, LER and MER data sets and an additional 1% uncorrelated uncertainty for each data set. The ZEUS97 data set has an independent luminosity uncertainty of 1.5%.

III. MONTE CARLO SAMPLES

The event selection is based primarily on finding a candidate scattered electron, a well-reconstructed event vertex and longitudinal energy-momentum balance. Neutral current (NC) DIS events are selected with high efficiency in the kinematic range under study. Background events arise predominantly from photoproduction ($Q^2 \approx 0$) where the scattered electron goes down the beam pipe and other particles are falsely identified as the scattered electron. Other background processes include non-DIS events producing high energy scattered electrons, such as QED-Compton scattering. Sufficient numbers of signal and background events have been simulated in order to design the analysis, understand the acceptance and evaluate remaining background levels.

The DIS signal processes were simulated using the DJANGOH 1.6 Monte Carlo (MC) model [30]. DJANGOH

[1]Here and in the following the term electron denotes generically both the electron and the positron.

[2]The ZEUS coordinate system is a right-handed Cartesian system, with the Z axis pointing in the proton beam direction, referred to as the forward direction, and the X axis pointing towards the center of HERA. The coordinate origin is at the center of the CTD.

is an interface of the MC programs HERACLES [30,31] and LEPTO [32]. Alternatively, parton cascades can be generated with the help of ARIADNE [33]. In this analysis, the CTEQ5D [34] parametrizations of the proton PDF were used and the hadronic final state was simulated with the color-dipole model of ARIADNE 4.12 [33]. Photoproduction events ($Q^2 < 1.5$ GeV^2), which are the largest background for the measurement, were simulated using the PYTHIA 6.221 [35] MC model in conjunction with the GRV-G-96 HO [36] parametrization of the photon PDF and with the CTEQ5D parametrization of the proton PDF. Additional background components that were considered were elastic QED Compton (QEDC) scattering and misreconstructed low-Q^2 DIS events, simulated using the GRAPE-COMPTON [37] and DJANGOH 1.6 MC models, respectively. The misreconstruction of low-Q^2 events occurs when a hadron is misidentified as a scattered electron. For all DJANGOH- and PYTHIA-generated samples the Lund string model of JETSET 7.4 [38] was used for the hadronization. The ZEUS detector response was simulated using a program based on GEANT 3.21 [39]. The generated events were passed through the detector simulation, subjected to the same trigger requirements as the data and processed by the same reconstruction programs.

The DJANGOH and PYTHIA samples included a diffractive component and first-order electroweak corrections. The diffractive and nondiffractive components of the DJANGOH sample were scaled (reweighted) to improve the description of the $\eta_{\max}$ distribution, where $\eta_{\max}$ is equal to the pseudorapidity of the most forward CAL energy deposit.

The electroweak corrections were simulated using the HERACLES 4.6 MC model. Their uncertainty was evaluated by comparing the predictions from HERACLES to the higher-order predictions from HECTOR 1.0 [40]. The predictions were found to agree within 0.5% and the remaining uncertainty was not included in the systematic uncertainties on the cross sections.

The predicted photoproduction backgrounds were compared with photoproduction data selected using the 6 m-Tagger and a photoproduction-enriched sample, separately for all three data sets, HER, LER and MER [41]. An event weight was determined for this background as a function of the candidate electron energy to bring the MC in agreement with the data. The same weighting function was found to suffice for all data sets. The weight reduced from 1.2 at electron-candidate energy of 6 GeV to 1.0 at electron-candidate energy of 10 GeV. A remaining uncertainty of $\pm 10\%$ in the photoproduction background was accounted for in the systematic uncertainties.

IV. VERTEX DISTRIBUTION

Events were separately analyzed for two different vertex regions: the central-vertex region, $|Z_{\text{vtx}}| < 30$ cm, and the shifted-vertex region, $30 < Z_{\text{vtx}} < 100$ cm. The latter region contained fewer events, but the scattered electrons from these events had a greatly increased geometrical acceptance at low Q^2.

The distribution of event vertices depended on the bunch structure of the proton and electron beams. Primary bunches were separated by 96 ns, whereas secondary electron bunches occurred at 2 ns intervals and secondary proton bunches occurred at 4.8 ns intervals. Assuming that one of the interacting particles was in a primary bunch, nine separate peaks of the vertex distribution along the Z direction, within ± 100 cm of the nominal interaction point, were produced. Event vertices originating from collisions of at least one particle not from a primary bunch are termed "satellite vertices."

A dedicated analysis of the vertex distributions using separate data sets was performed, leading to a parametrization with ten Gaussian functions, two Gaussian functions being required to fit the central peak [41]. The obtained efficiency-corrected Z_{vtx} distributions for the HER, MER and LER samples are shown in Fig. 1.

The vertex distributions of the MC samples were accurately tuned to match the distributions in the data. This was particularly crucial to obtain proper acceptance corrections for the events selected in the two different vertex regions. The underlying vertex distributions were extracted using a number of different data selections, leading to the determination of an increased uncorrelated normalization uncertainty for the shifted-vertex region of 3.0%.

V. EVENT RECONSTRUCTION AND SELECTION

The event kinematics were evaluated based on the reconstruction of the scattered electron [42] using

$$y_e = 1 - \frac{E'_e}{2E_e}(1 - \cos\theta_e), \tag{2}$$

$$Q^2_e = 2E'_e E_e (1 + \cos\theta_e), \tag{3}$$

where θ_e and E'_e are the polar angle and energy of the scattered electron, respectively.

Electrons were identified using a neural network based on the moments of the three-dimensional shower profile of clusters found in the CAL [43]. The quantity E'_e was reconstructed using the CAL and θ_e was determined using the reconstructed interaction vertex and scattered-electron position in the SRTD or, if outside the SRTD acceptance, in the RHES. In less than 2% of events, θ_e could not be determined in this way; such events were rejected.

The quantity $\delta \equiv \sum_i (E - p_Z)_i = \sum_i (E - E\cos\theta)_i$ was used both in the trigger and in the off-line analysis. The sum runs over all CAL energy deposits. Conservation of energy, E, and longitudinal momentum, p_Z, implies that $\delta \approx 2E_e = 55$ GeV. Undetected particles that escape

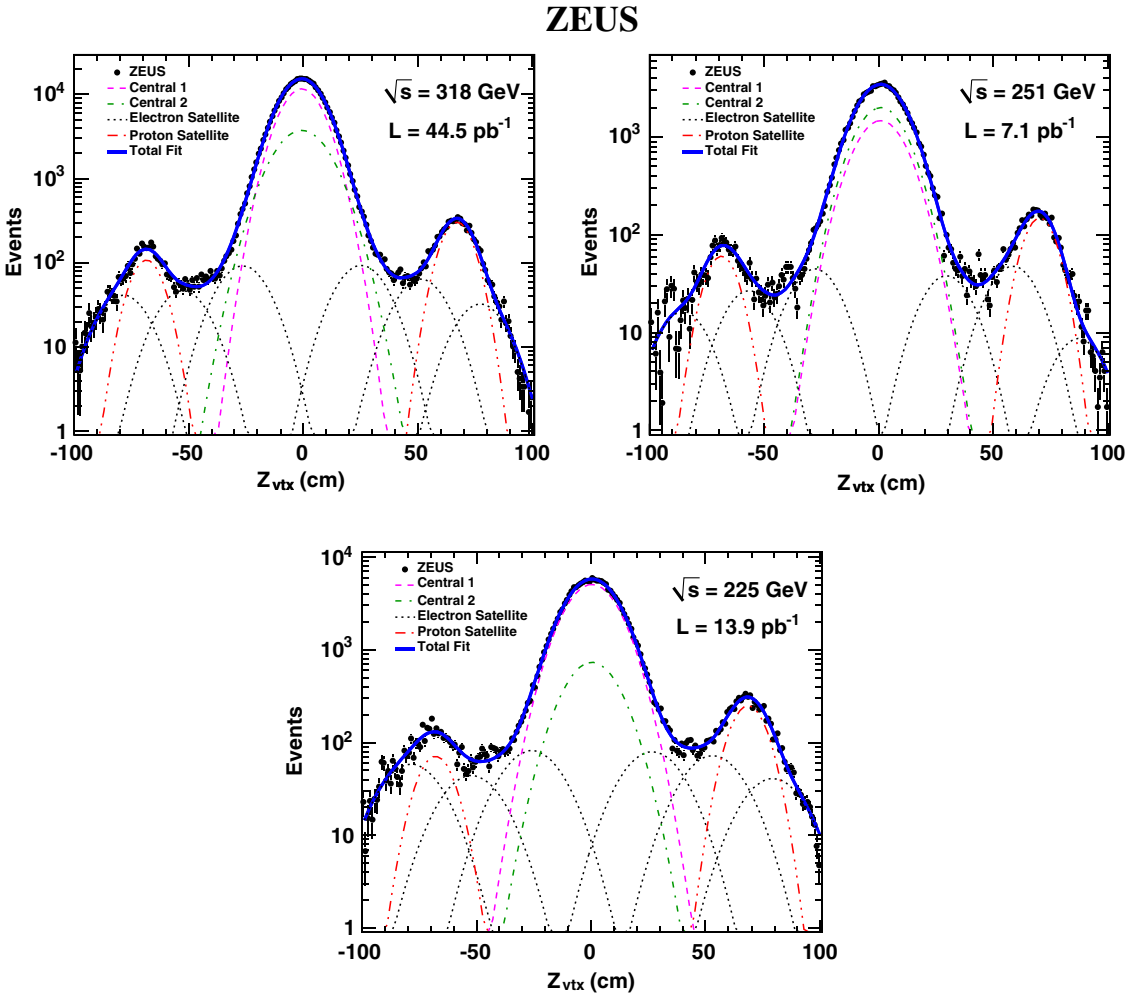

FIG. 1 (color online). Efficiency-corrected Z_{vtx} distribution for the HER, MER and LER data sets. A sum of several contributions is fitted to the data: six Gaussian functions representing electron satellite peaks, two Gaussians representing proton satellite peaks and two Gaussians for central vertex events. The fitted individual contributions are shown (dotted, dash-dotted and dashed curves) as well as the total fit (solid curve).

through the forward beam-pipe hole contribute negligibly to δ. Undetected particles that escape through the rear beam-pipe hole, such as the final-state electron in a photoproduction event, cause a substantial reduction in δ. Events not originating from ep collisions often exhibit a very large δ.

A three-level trigger system was used to select events online [20,44–46]. A dedicated trigger was developed providing high efficiency for high-y events [47]. The trigger required an event to have $\delta > 30$ GeV and either an electron candidate with $E' > 4$ GeV in the RCAL outside a 30×30 cm^2 box centered around the beam pipe, or a $\delta^{\theta<165^\circ} > 20$ GeV, where $\delta^{\theta<165^\circ}$ denotes δ calculated only from the CAL energy deposits at polar angles less than 165°. The electron energy requirement was reduced to $E' > 2$ GeV for the MER and LER data runs.

Events were selected off-line if:

(i) $42 < \delta < 65$ GeV;

(ii) the reconstructed interaction vertex fulfilled $|Z_{\mathrm{vtx}}| < 30$ cm for the central- and $30 < Z_{\mathrm{vtx}} < 100$ cm for the shifted-vertex region;

(iii) the energy of the electron candidate satisfied $E'_e > 6$ GeV;

(iv) the event topology was not compatible with an elastic QEDC scattering event, which has an event signature of two, and only two, electromagnetic deposits back to back in azimuthal angle;

(v) the event timing was consistent with that of an ep interaction;

(vi) $y_e < 0.95$ and $y_{\mathrm{JB}} > 0.05$, where y_{JB} is the Jacquet-Blondel estimator [48] of y;

(vii) $p_{T,h}/p_{T,e} > 0.3$, where $p_{T,h}$ and $p_{T,e}$ refer to the transverse momentum of the hadronic system and electron candidate, respectively.

The projected path of the electron candidate was required to:

(i) exit the CTD at a radius > 20 cm and hence traverse the MVD fiducial volume (typically three active layers) and at least four active layers of the CTD;
(ii) enter the RCAL at a radius < 135 cm, to ensure full energy containment in the RCAL.

Hit information from the MVD and CTD was used to validate electron candidates [47]. The procedure was based on the ratios of the number of observed to the maximum number of possible hits in the MVD and CTD along the track trajectory, denoted $f_{\rm hit}^{\rm MVD}$ and $f_{\rm hit}^{\rm CTD}$. The requirements

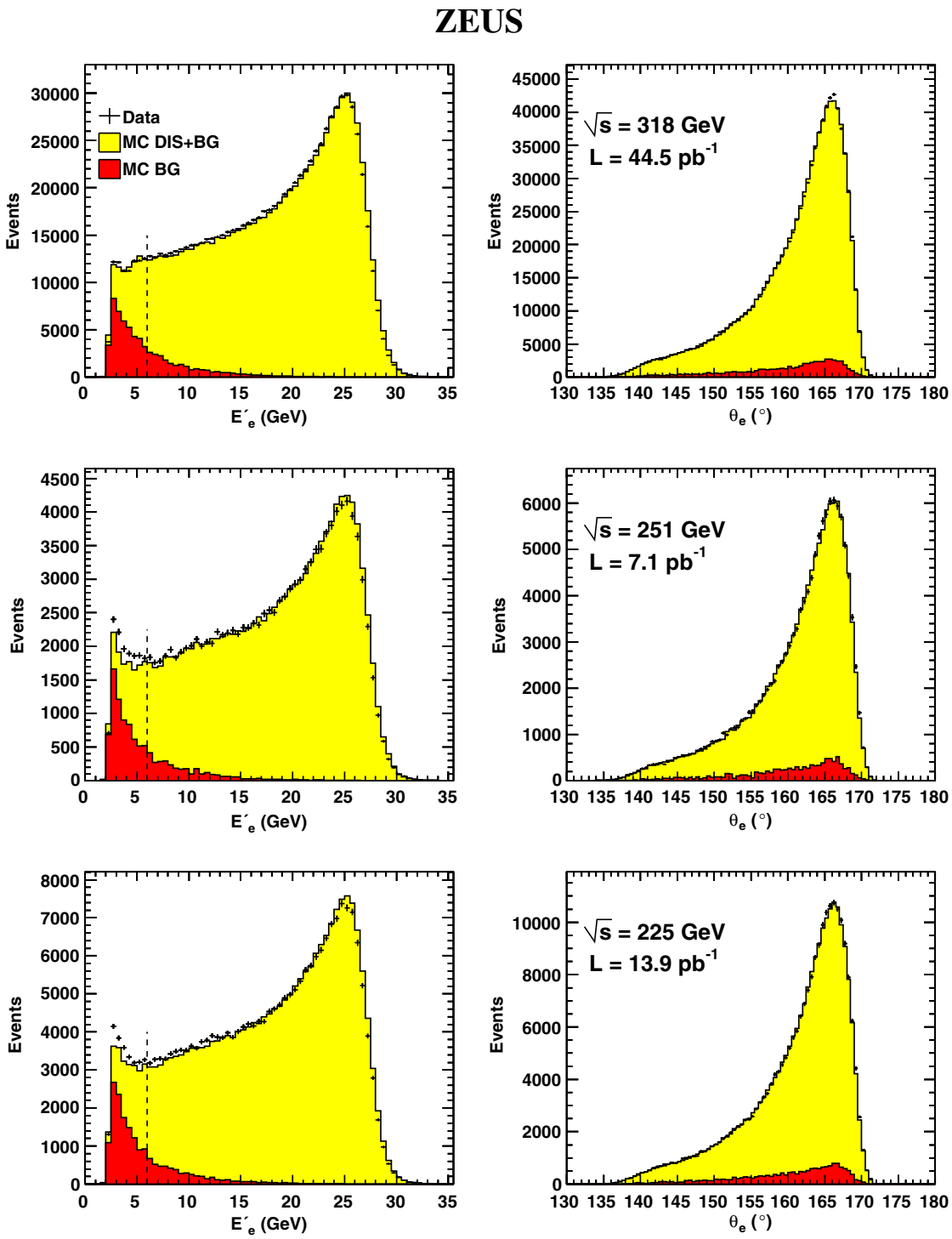

FIG. 2 (color online). Detector-level distributions of the variables E'_e and θ_e for the $|Z_{\rm vtx}| < 30$ cm region for the HER, MER and LER data sets, compared to the combined MC predictions (MC DIS + BG). The background-only MC is labeled MC BG. The vertical dashed line indicates the lower limit on the scattered-electron energy used in this analysis. The θ_e distributions are shown for $E'_e > 6$ GeV.

on the ratios were $f_{\rm hit}^{\rm MVD} > 0.45$ and $f_{\rm hit}^{\rm CTD} > 0.6$. This method was used to increase the polar-angle acceptance compared to the regular tracking capability of the MVD + CTD [41]. The efficiency of this selection was studied in data and MC using specially selected data sets. A reweighting of the MC for the central-vertex event sample was found to be necessary for electrons at small scattering angles, with a maximum weight of 1.06 for the smallest

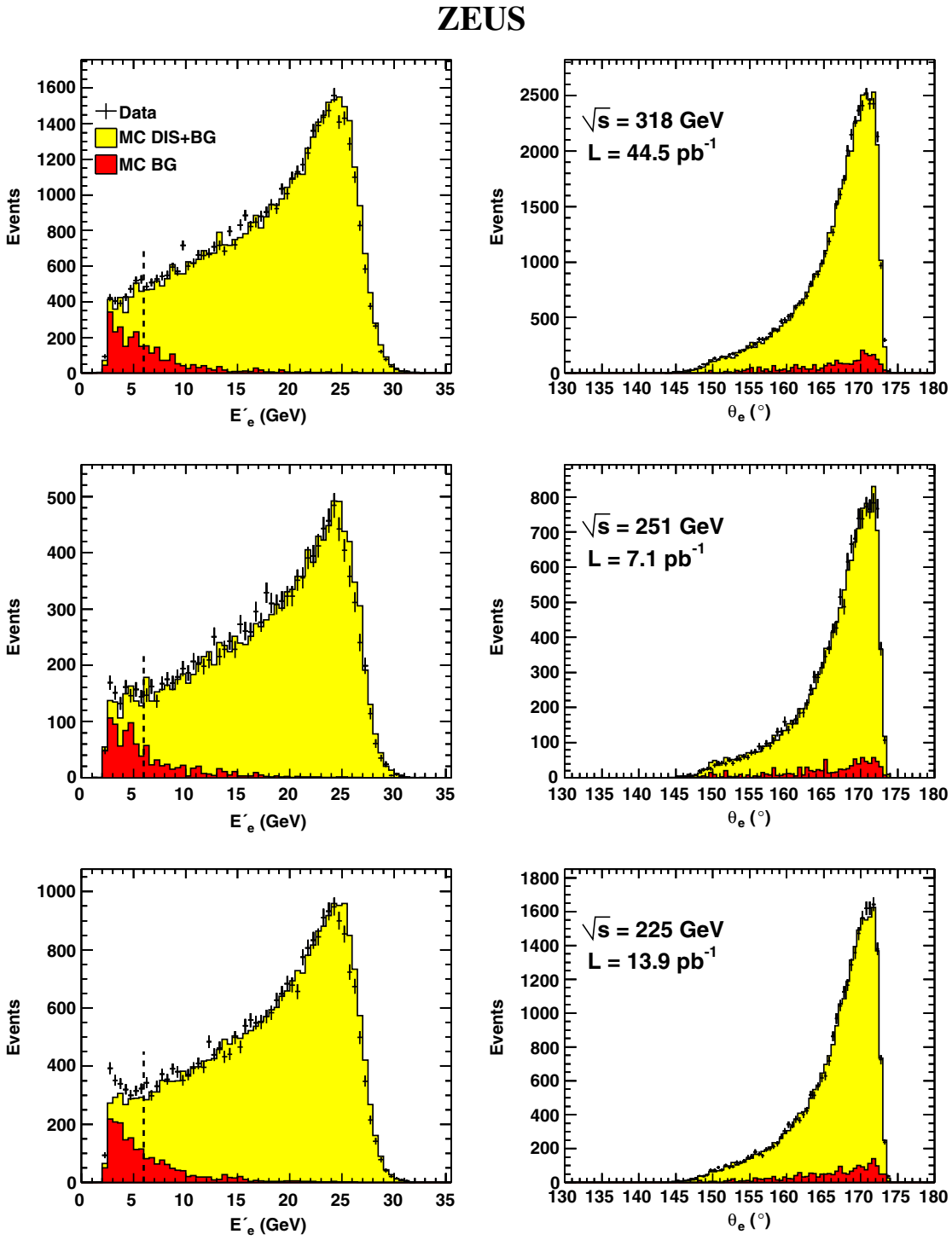

FIG. 3 (color online). Detector-level distributions of the variables E'_e and θ_e for the $30 < Z_{\rm vtx} < 100$ cm region for the HER, MER and LER data sets, compared to the combined MC predictions (MC DIS + BG). The background-only MC is labeled MC BG. The vertical dashed line indicates the lower limit on the scattered-electron energy used in this analysis. The θ_e distributions are shown for $E'_e > 6$ GeV.

angles used in this analysis. The uncertainty on this reweighting procedure was included in the systematic uncertainties. No reweighting was necessary for the shifted-vertex events, as the efficiency of the selection is high and uniform for this sample.

Figures 2 and 3 show the distributions of the variables E'_e and θ_e for the HER, MER and LER data sets compared to the combined detector-level predictions from the MC models, for the central- and shifted-vertex events. In the region $E'_e > 6$ GeV, which is relevant for the analysis, the agreement is adequate for the extraction of the cross sections. According to the MC models, the final data samples contained 97% DIS signal and 3% background events for both the central- and shifted-vertex data samples in all data sets. The vast majority of the background events were found at low Q^2 and high y and resulted from photoproduction processes. In the kinematic bin most affected the background fraction was 30%.

VI. CROSS-SECTION MEASUREMENTS

The reduced cross section at a given (x, Q^2) value was evaluated from the number of events reconstructed in a bin according to

$$\tilde{\sigma}(x, Q^2) = \frac{N_{\text{data}} - N_{\text{MC}}^{\text{bg}}}{N_{\text{MC}}^{\text{DIS}}} \tilde{\sigma}_{\text{SM}}(x, Q^2). \quad (4)$$

Here N_{data}, $N_{\text{MC}}^{\text{bg}}$ and $N_{\text{MC}}^{\text{DIS}}$ denote, respectively, the number of observed events in the data and the expected number of background and signal DIS events. The latter two numbers were taken from the MC simulations normalized to the data luminosity. The quantity $\tilde{\sigma}_{\text{SM}}(x, Q^2)$ denotes the standard model electroweak Born-level reduced cross section and was calculated with the DJANGOH simulation with electroweak corrections switched off.

The reduced cross sections were measured according to Eq. (4) for kinematic values in the ranges $0.13 \leq y \leq 0.75$

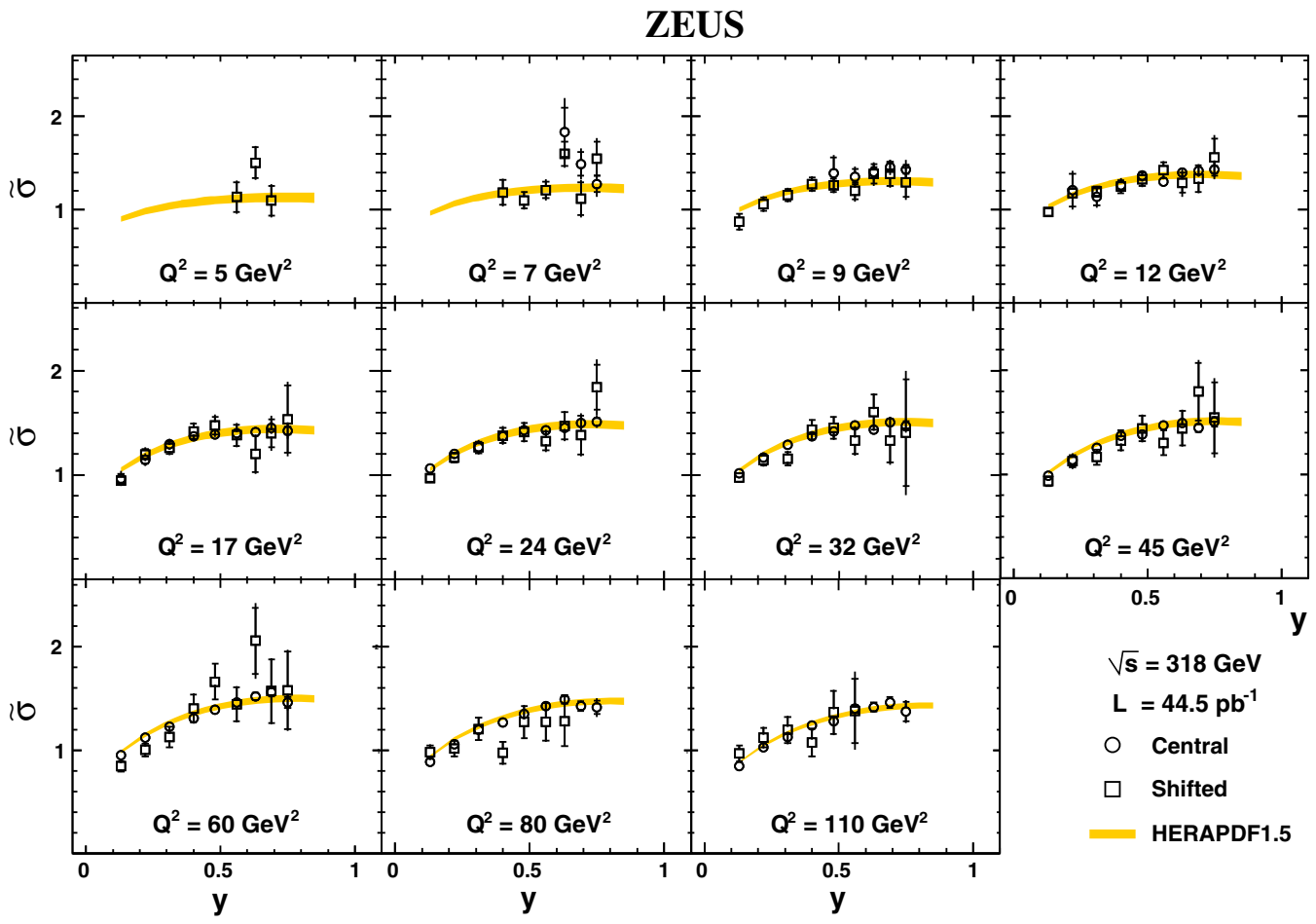

FIG. 4 (color online). The reduced cross sections, $\tilde{\sigma}$, for $\sqrt{s} = 318$ GeV, at 11 values of Q^2 as a function of y. The central- and shifted-vertex data results are shown as circles and squares, respectively. The inner error bars correspond to the statistical uncertainty, while the outer error bars represent the statistical and systematic uncertainties added in quadrature. Next-to-next-to-leading-order (NNLO) QCD predictions from HERAPDF1.5 are also shown. The bands indicate the uncertainty in the predictions.

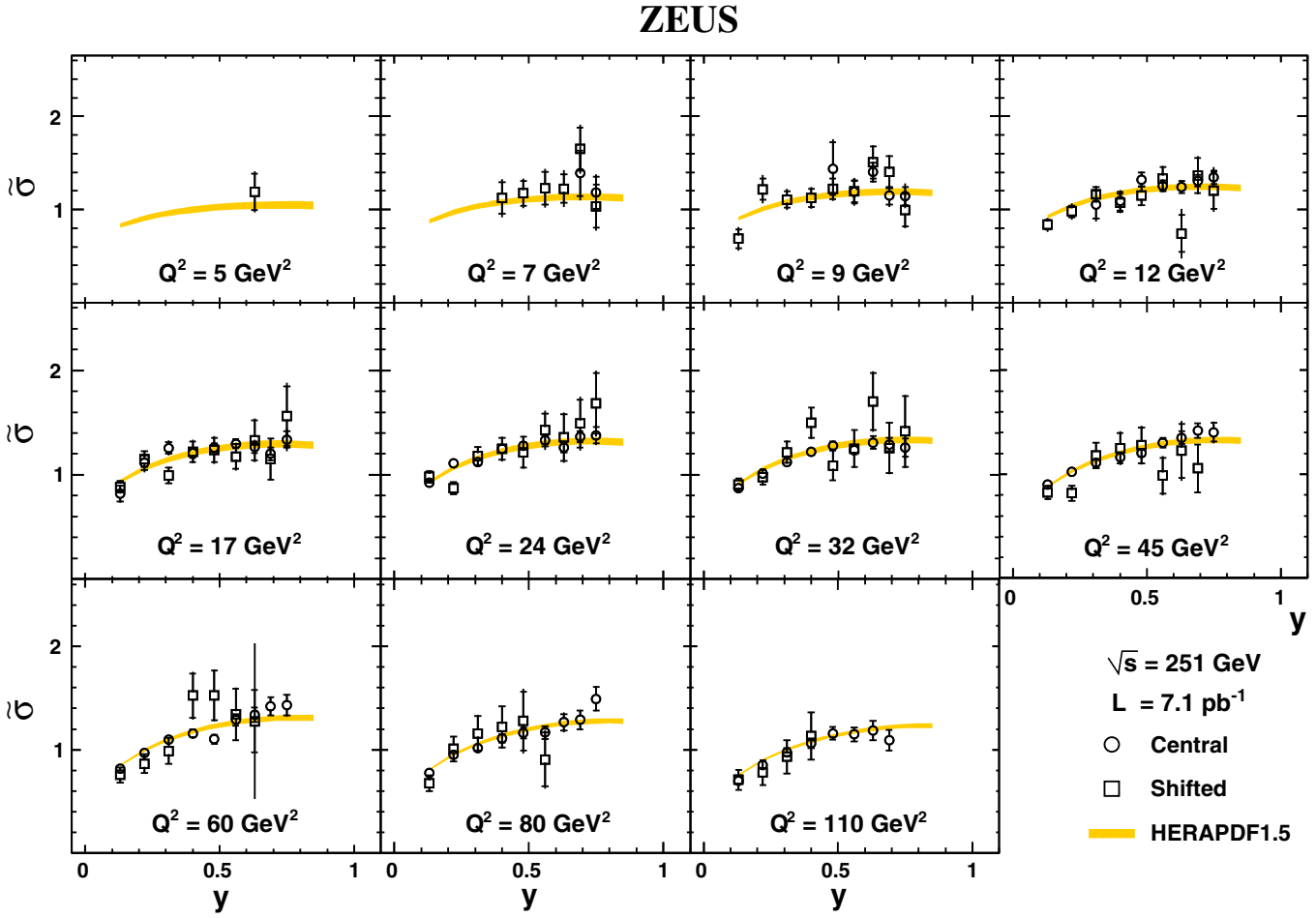

FIG. 5 (color online). The reduced cross sections, $\tilde{\sigma}$, for $\sqrt{s} = 251$ GeV, at 11 values of Q^2 as a function of y. The central- and shifted-vertex data results are shown as circles and squares, respectively. The inner error bars correspond to the statistical uncertainty, while the outer error bars represent the statistical and systematic uncertainties added in quadrature. NNLO QCD predictions from HERAPDF1.5 are also shown. The bands indicate the uncertainty in the predictions.

and $5 \leq Q^2 \leq 110$ GeV^2. They were measured separately for the central- and shifted-vertex regions, referred to as $\tilde{\sigma}_{\text{cen}}$ and $\tilde{\sigma}_{\text{sh}}$. The following y-bin boundaries were used for the measurement: 0.090, 0.175, 0.265, 0.355, 0.440, 0.520, 0.600, 0.660, 0.720, 0.780, together with the following Q^2-bin boundaries: 4.5, 6, 8, 11, 15, 20, 28, 38, 52, 70, 95, 130 GeV^2. Figures 4–6 show the obtained cross sections at fixed values of Q^2 as functions of y for the HER, MER and LER samples, separately for the central- and shifted-vertex regions. Reasonable agreement is observed between them. The predictions based on the HERAPDF1.5 PDF set [49] are also depicted in the Figs. 4–6 and provide a good description of the data. The reduced cross sections are reported in Tables I–VI for central- and shifted-vertex regions and are used for the extraction of structure functions.

VII. SYSTEMATIC UNCERTAINTIES

A number of possible effects that could affect the cross-section measurements have been investigated. These are classified according to whether they affect measurements in a correlated way, can be treated as uncorrelated, or are negligibly small. The systematic uncertainties are denoted with the symbols δ_{source}. The numbers in the parentheses give an indication of the typical values observed in the cross-section bins and the maximum observed value. The correlated systematic uncertainties are:

(i) $\{\delta_{\gamma p}\}$, the $\pm 10\%$ normalization uncertainty on the level of photoproduction background (0.5%, 3%);
(ii) $\{\delta_{E_{\text{had}}}\}$, the $\pm 2\%$ hadronic-energy-scale uncertainty, evaluated by varying the scale in simulated events (0.5%, 4%);
(iii) $\{\delta_{\text{diff}}\}$, the uncertainty on the scale factors applied to the diffractive DJANGOH component (0.2%, 0.5%);
(iv) $\{\delta_{\text{hits}}\}$, the electron validation using CTD and MVD information (1%, 2%).

These δ_{source} values are listed in Tables I–VI for the reduced cross sections at the three different center-of-mass energies. The reduced cross-section changes are quoted with a sign indicating how they should be handled in a fit; positive

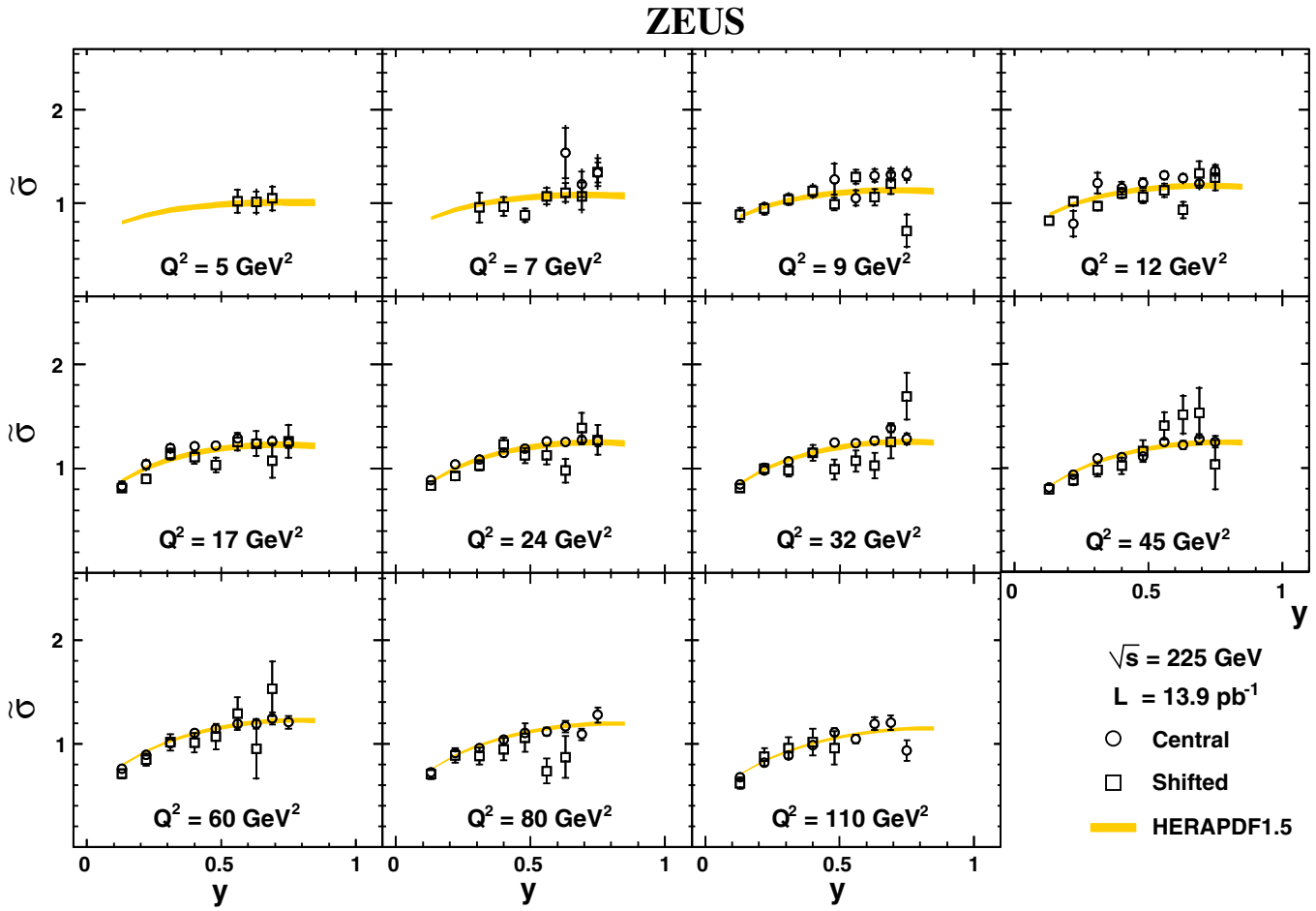

FIG. 6 (color online). The reduced cross sections, $\tilde{\sigma}$, for $\sqrt{s} = 225$ GeV, at 11 values of Q^2 as a function of y. The central- and shifted-vertex data results are shown as circles and squares, respectively. The inner error bars correspond to the statistical uncertainty, while the outer error bars represent the statistical and systematic uncertainties added in quadrature. NNLO QCD predictions from HERAPDF1.5 are also shown. The bands indicate the uncertainty in the predictions.

quantities indicate an increase in the cross sections, while negative quantities indicate a decrease. The probability distributions for the cross sections are taken to be Gaussian. The quoted numbers in the table correspond to variations of one standard deviation.

A number of systematic tests produced sizable changes in the extracted cross sections, but should be considered as uncorrelated in fits to the cross sections. These are:

(i) $\{\delta_{E_e}\}$, the electron-energy-scale uncertainty [14] of $\pm 0.5\%$ for $E'_e > 20$ GeV, increasing to $\pm 1.9\%$ at $E'_e = 6$ GeV, evaluated by varying the scale in simulated events (1%, 5%);

(ii) $\{\delta_{eID}\}$, the uncertainty of the electron-finding efficiency, evaluated by loosening or tightening the criterion applied to the output of the neural network used to select electron candidates, both for data and MC (0.2%, 5%);

(iii) $\{\delta_{\mathrm{Zvtx}}\}$, the uncertainty on the Z_{vtx} distribution, that was evaluated by varying the event-selection criteria used in the extraction of the distribution (0.5%, 10%);

(iv) $\{\delta_{dx}, \delta_{dy}\}$, the SRTD and HES position uncertainty of ± 2 mm in both the horizontal and vertical directions (0.5%, 4%).

These uncertainties are combined in quadrature for each bin and quoted under the label δ_{unc}. This uncertainty also includes the statistical uncertainty in the MC sample.

Finally, a number of checks were performed with resulting cross-section variations small enough that they are considered negligible. These include:

(i) the trigger-efficiency uncertainty;

(ii) the uncertainty due to the electroweak corrections. In a separate analysis [50] the differential cross sections for radiating an initial-state photon were also extracted. These results are in excellent agreement with the expectations from HERACLES, adding confidence that the radiative effects are well simulated.

In addition to the uncertainties listed above, the normalization uncertainties for the different data sets are:

(i) a correlated luminosity uncertainty of 1.5% for the HER, MER and LER cross sections;

(ii) an additional uncorrelated luminosity and vertex-distribution uncertainty of 1.0% for the central-vertex HER, MER and LER cross sections and 3.0% for the shifted-vertex cross sections.

The total systematic uncertainty, $\delta_{\rm sys}$, in each bin formed by adding the individual uncertainties in quadrature, is also given in Tables I–VI. The total systematic uncertainties in the tables do not include the normalization uncertainty.

TABLE I. The reduced cross sections, $\tilde{\sigma}$, for the reaction $e^+p \to e^+X$ at $\sqrt{s} = 318$ GeV for the central-vertex region. The first three columns contain the bin centers in Q^2, x, and y, and the next four contain the measured cross section, the statistical uncertainty, total systematic uncertainty and the uncorrelated uncertainty, respectively. The final four list the bin-to-bin correlated uncertainties from each systematic source, $\delta_{\gamma p}$, $\delta_{E_{\rm had}}$, $\delta_{\rm diff}$, $\delta_{\rm hits}$. The normalization uncertainty (see Sec. VII) is not included.

Q^2 (GeV^2)	x	y	$\tilde{\sigma}$ HER	$\delta_{\rm stat}$ (%)	$\delta_{\rm sys}$ (%)	$\delta_{\rm unc}$ (%)	$\delta_{\gamma p}$ (%)	$\delta_{E_{\rm had}}$ (%)	$\delta_{\rm diff}$ (%)	$\delta_{\rm hits}$ (%)
7	0.000110	0.63	1.810	10.05	17.30	16.70	0.00	−4.09	−0.61	1.83
7	0.000100	0.69	1.470	5.39	10.06	9.63	−0.97	−1.69	−0.56	2.06
7	0.000092	0.75	1.257	3.45	10.20	7.36	−3.14	−5.86	−0.63	2.29
9	0.000185	0.48	1.372	8.67	10.84	10.62	−0.57	−0.70	−0.10	1.99
9	0.000159	0.56	1.334	4.25	6.32	5.95	−0.61	0.32	−0.25	2.00
9	0.000141	0.63	1.382	2.68	5.09	4.57	−0.44	−1.05	−0.42	1.89
9	0.000129	0.69	1.434	1.98	5.14	3.84	−1.23	−2.52	−0.51	1.90
9	0.000119	0.75	1.419	1.72	6.77	4.54	−2.51	−3.86	−0.58	1.90
12	0.000539	0.22	1.196	10.66	13.24	13.13	0.00	0.45	0.09	1.68
12	0.000383	0.31	1.124	6.16	7.98	7.76	0.00	−0.13	0.04	1.86
12	0.000297	0.40	1.239	3.43	4.95	4.55	−0.03	−0.48	−0.20	1.89
12	0.000247	0.48	1.340	2.16	4.05	3.50	−0.44	−0.59	−0.16	1.90
12	0.000212	0.56	1.279	1.55	3.27	2.47	−0.81	−0.61	−0.28	1.86
12	0.000188	0.63	1.384	1.44	3.36	2.42	−0.89	−1.21	−0.38	1.74
12	0.000172	0.69	1.404	1.34	3.80	2.47	−1.29	−1.96	−0.40	1.63
12	0.000158	0.75	1.416	1.45	5.86	3.53	−2.58	−3.56	−0.52	1.54
17	0.001293	0.13	0.954	3.65	6.45	6.11	0.00	−0.75	0.09	1.91
17	0.000764	0.22	1.129	2.47	4.08	3.60	0.00	−0.24	0.10	1.89
17	0.000542	0.31	1.272	1.68	3.10	2.49	−0.03	−0.30	−0.10	1.83
17	0.000420	0.40	1.353	1.29	2.42	1.65	−0.08	−0.20	−0.18	1.75
17	0.000350	0.48	1.373	1.13	2.31	1.54	−0.23	−0.29	−0.21	1.67
17	0.000300	0.56	1.389	1.03	2.28	1.51	−0.42	−0.55	−0.24	1.55
17	0.000267	0.63	1.402	1.21	2.65	1.72	−0.92	−1.01	−0.35	1.44
17	0.000244	0.69	1.440	1.30	3.77	2.46	−1.45	−2.08	−0.37	1.28
17	0.000224	0.75	1.409	1.48	5.22	3.11	−2.08	−3.46	−0.46	1.05
24	0.001826	0.13	1.048	0.98	2.88	2.16	0.00	−0.72	0.08	1.76
24	0.001079	0.22	1.190	0.86	2.61	1.98	−0.00	−0.21	−0.04	1.69
24	0.000766	0.31	1.257	0.81	1.98	1.14	−0.06	−0.15	−0.09	1.61
24	0.000593	0.40	1.360	0.81	1.77	0.91	−0.09	−0.19	−0.14	1.50
24	0.000494	0.48	1.422	0.83	1.75	1.00	−0.28	−0.27	−0.16	1.38
24	0.000424	0.56	1.416	0.88	1.73	1.05	−0.37	−0.52	−0.24	1.20
24	0.000377	0.63	1.440	1.10	2.21	1.53	−0.65	−1.01	−0.25	1.02
24	0.000344	0.69	1.485	1.24	3.57	2.89	−1.08	−1.55	−0.28	0.83
24	0.000316	0.75	1.495	1.42	3.78	2.25	−1.80	−2.36	−0.36	0.58
32	0.002434	0.13	1.013	0.64	2.36	1.69	−0.00	−0.62	0.06	1.52
32	0.001438	0.22	1.163	0.66	2.13	1.57	−0.00	−0.19	−0.03	1.42
32	0.001021	0.31	1.280	0.71	1.51	0.76	−0.02	−0.13	−0.09	1.30
32	0.000791	0.40	1.358	0.79	1.61	1.07	−0.09	−0.26	−0.13	1.16
32	0.000659	0.48	1.407	0.89	1.44	0.99	−0.19	−0.18	−0.18	1.00
32	0.000565	0.56	1.462	1.00	1.62	1.25	−0.39	−0.47	−0.20	0.81
32	0.000502	0.63	1.419	1.29	1.96	1.49	−0.61	−0.90	−0.25	0.60
32	0.000459	0.69	1.490	1.39	2.62	1.93	−0.69	−1.56	−0.24	0.40
32	0.000422	0.75	1.453	1.67	4.03	2.97	−1.90	−1.92	−0.29	0.21
45	0.003423	0.13	0.981	0.58	1.89	1.31	0.00	−0.65	0.08	1.21
45	0.002023	0.22	1.128	0.64	1.92	1.57	−0.01	−0.15	−0.02	1.08
45	0.001435	0.31	1.243	0.73	1.22	0.76	−0.00	−0.12	−0.09	0.94
45	0.001112	0.40	1.357	0.85	1.44	1.19	−0.03	−0.16	−0.13	0.78

(Table continued)

TABLE I. (*Continued*)

Q^2 (GeV^2)	x	y	$\tilde{\sigma}$ HER	δ_{stat} (%)	δ_{sys} (%)	δ_{unc} (%)	$\delta_{\gamma p}$ (%)	$\delta_{E_{\text{had}}}$ (%)	δ_{diff} (%)	δ_{hits} (%)
45	0.000927	0.48	1.372	1.00	1.40	1.24	−0.10	−0.14	−0.18	0.62
45	0.000795	0.56	1.454	1.11	1.74	1.53	−0.28	−0.63	−0.17	0.43
45	0.000706	0.63	1.481	1.43	2.27	2.11	−0.52	−0.59	−0.20	0.26
45	0.000645	0.69	1.431	1.62	3.07	2.69	−1.03	−1.06	−0.23	−0.13
45	0.000593	0.75	1.491	1.79	3.48	2.85	−1.38	−1.43	−0.27	−0.02
60	0.004564	0.13	0.939	0.66	1.73	1.39	0.00	−0.58	0.10	0.85
60	0.002697	0.22	1.108	0.74	1.72	1.56	−0.00	−0.13	0.02	0.73
60	0.001914	0.31	1.216	0.86	1.04	0.86	−0.00	−0.07	−0.09	0.58
60	0.001483	0.40	1.298	1.01	1.45	1.38	−0.04	−0.11	−0.08	0.43
60	0.001236	0.48	1.379	1.17	1.32	1.26	−0.09	−0.21	−0.17	0.28
60	0.001060	0.56	1.446	1.31	1.48	1.41	−0.22	−0.32	−0.23	−0.14
60	0.000942	0.63	1.505	1.68	2.51	2.31	−0.46	−0.82	−0.26	−0.05
60	0.000860	0.69	1.543	1.82	2.53	2.20	−0.44	−1.15	−0.25	−0.01
60	0.000791	0.75	1.445	2.17	4.64	3.70	−1.55	−2.33	−0.27	0.00
80	0.006085	0.13	0.875	0.76	1.58	1.36	0.00	−0.61	0.14	0.49
80	0.003596	0.22	1.044	0.85	1.53	1.47	0.00	−0.13	0.03	0.38
80	0.002552	0.31	1.185	0.98	1.02	0.98	−0.01	0.04	−0.04	0.26
80	0.001978	0.40	1.257	1.17	1.39	1.38	−0.05	0.06	−0.07	0.15
80	0.001648	0.48	1.336	1.35	1.36	1.34	−0.07	0.16	−0.12	−0.06
80	0.001413	0.56	1.414	1.50	1.92	1.83	−0.24	−0.52	−0.16	−0.01
80	0.001256	0.63	1.477	1.91	2.19	2.13	−0.32	−0.36	−0.23	0.00
80	0.001147	0.69	1.413	2.19	2.74	2.55	−0.65	−0.73	−0.16	0.00
80	0.001055	0.75	1.397	2.55	6.08	5.67	−1.41	−1.67	−0.20	0.00
110	0.008367	0.13	0.834	0.88	1.50	1.36	0.00	−0.57	0.19	0.19
110	0.004944	0.22	1.019	0.99	1.76	1.75	−0.00	−0.12	0.03	−0.12
110	0.003509	0.31	1.117	1.17	1.15	1.14	−0.01	−0.10	−0.03	−0.05
110	0.002719	0.40	1.226	1.36	1.46	1.45	−0.03	−0.14	−0.08	−0.01
110	0.002266	0.48	1.265	1.61	2.22	2.20	−0.11	−0.24	−0.12	0.00
110	0.001942	0.56	1.386	1.81	2.21	2.13	−0.38	−0.43	−0.12	0.00
110	0.001727	0.63	1.402	2.25	2.65	2.63	−0.12	−0.26	−0.11	0.00
110	0.001576	0.69	1.447	2.57	3.19	3.08	−0.46	−0.66	−0.13	0.00
110	0.001450	0.75	1.358	4.14	6.90	6.74	−1.16	−0.88	−0.25	0.00

TABLE II. The reduced cross sections, $\tilde{\sigma}$, for the reaction $e^+p \to e^+X$ at $\sqrt{s} = 318$ GeV for the shifted-vertex region. Further details are as described in the caption of Table I.

Q^2 (GeV^2)	x	y	$\tilde{\sigma}$ HER	δ_{stat} (%)	δ_{sys} (%)	δ_{unc} (%)	$\delta_{\gamma p}$ (%)	$\delta_{E_{\text{had}}}$ (%)	δ_{diff} (%)	δ_{hits} (%)
5	0.000088	0.56	1.134	10.30	11.78	11.68	−0.55	−1.06	−0.13	0.97
5	0.000078	0.63	1.503	7.34	9.60	9.50	−0.40	0.73	−0.22	1.08
5	0.000072	0.69	1.096	8.96	13.47	12.82	−1.74	−3.50	−0.41	1.26
7	0.000173	0.40	1.185	8.02	9.73	9.67	−0.34	0.44	0.01	0.87
7	0.000144	0.48	1.101	6.07	6.50	6.39	−0.19	−0.53	−0.04	1.03
7	0.000124	0.56	1.210	5.40	7.79	7.68	−0.32	0.72	−0.23	1.06
7	0.000110	0.63	1.598	5.73	7.54	7.45	−0.10	0.58	−0.22	1.02
7	0.000100	0.69	1.117	7.69	16.42	16.17	−2.42	−0.74	−0.39	1.26
7	0.000092	0.75	1.546	7.29	12.57	11.88	−1.51	−3.63	−0.30	1.16
9	0.000685	0.13	0.870	7.37	8.00	7.95	0.00	−0.35	0.02	0.80
9	0.000405	0.22	1.060	4.99	6.17	6.09	0.00	−0.44	−0.16	0.90
9	0.000287	0.31	1.157	4.19	5.37	5.27	0.00	0.07	0.08	1.00
9	0.000222	0.40	1.274	4.09	5.00	4.89	0.00	0.18	−0.14	1.01
9	0.000185	0.48	1.261	4.29	5.28	5.15	−0.19	−0.58	−0.06	1.02
9	0.000159	0.56	1.199	4.82	8.03	7.93	−0.62	0.34	−0.05	1.08
9	0.000141	0.63	1.383	5.50	7.31	7.10	−0.45	−1.29	−0.08	1.05

(Table continued)

TABLE II. (*Continued*)

Q^2 (GeV^2)	x	y	$\tilde{\sigma}$ HER	δ_{stat} (%)	δ_{sys} (%)	δ_{unc} (%)	$\delta_{\gamma p}$ (%)	$\delta_{E_{\text{had}}}$ (%)	δ_{diff} (%)	δ_{hits} (%)
9	0.000129	0.69	1.385	6.08	8.80	8.63	−1.08	−0.64	−0.39	1.11
9	0.000119	0.75	1.293	7.54	12.59	12.09	−1.45	−2.98	−0.21	1.16
12	0.000913	0.13	0.972	3.14	4.15	3.94	0.00	−0.88	−0.02	1.00
12	0.000539	0.22	1.179	3.02	4.02	3.89	0.00	−0.14	0.04	1.00
12	0.000383	0.31	1.192	3.43	3.61	3.45	−0.02	−0.27	0.04	1.01
12	0.000297	0.40	1.247	3.86	4.36	4.22	−0.25	−0.20	−0.16	1.03
12	0.000247	0.48	1.325	4.21	4.81	4.70	−0.05	0.12	−0.07	1.01
12	0.000212	0.56	1.424	4.39	5.23	5.10	−0.16	−0.48	−0.12	1.02
12	0.000188	0.63	1.288	5.89	10.16	10.06	−0.69	0.61	−0.11	1.07
12	0.000172	0.69	1.335	6.86	9.47	9.24	−1.45	−0.91	−0.12	1.16
12	0.000158	0.75	1.562	7.61	13.34	11.59	−1.74	−6.25	−0.49	1.17
17	0.001293	0.13	0.946	2.90	3.60	3.39	0.00	−0.68	0.05	1.00
17	0.000764	0.22	1.199	3.08	4.84	4.72	0.00	−0.35	0.08	1.00
17	0.000542	0.31	1.258	3.48	3.82	3.68	−0.02	−0.04	−0.17	1.01
17	0.000420	0.40	1.419	3.88	4.80	4.68	0.00	0.34	−0.14	1.01
17	0.000350	0.48	1.473	4.34	6.02	5.92	−0.11	0.35	0.02	1.02
17	0.000300	0.56	1.381	5.20	6.47	6.33	−0.67	−0.28	−0.18	1.09
17	0.000267	0.63	1.200	7.41	14.06	13.90	−1.72	−0.27	−0.22	1.17
17	0.000244	0.69	1.398	7.22	9.61	9.52	−0.34	0.66	−0.40	1.03
17	0.000224	0.75	1.536	8.98	21.29	21.11	−2.27	−0.78	−0.09	1.25
24	0.001826	0.13	0.968	2.71	3.75	3.55	0.00	−0.67	0.12	1.00
24	0.001079	0.22	1.169	2.89	3.22	3.05	0.00	−0.12	0.02	1.01
24	0.000766	0.31	1.264	3.40	4.37	4.25	0.00	0.14	−0.01	1.00
24	0.000593	0.40	1.379	3.97	4.97	4.83	−0.16	0.46	−0.30	1.02
24	0.000494	0.48	1.413	4.62	5.22	5.11	0.00	0.26	0.01	1.01
24	0.000424	0.56	1.327	5.38	6.21	6.11	−0.08	−0.45	−0.25	1.02
24	0.000377	0.63	1.472	6.73	7.21	7.13	−0.28	0.15	−0.03	1.04
24	0.000344	0.69	1.385	8.27	12.20	11.63	−1.47	−3.17	−0.12	1.16
24	0.000316	0.75	1.843	7.69	12.39	12.31	−0.71	−0.45	−0.28	1.07
32	0.002434	0.13	0.976	3.16	3.70	3.48	0.00	−0.73	0.10	1.00
32	0.001438	0.22	1.145	3.53	4.57	4.46	0.00	0.04	−0.04	1.00
32	0.001021	0.31	1.159	4.25	4.49	4.37	0.00	0.08	−0.16	1.01
32	0.000791	0.40	1.435	4.79	4.92	4.81	0.00	0.27	−0.03	1.01
32	0.000659	0.48	1.451	5.41	5.55	5.45	0.00	−0.31	−0.10	1.00
32	0.000565	0.56	1.328	6.94	7.97	7.88	−0.43	0.29	−0.19	1.05
32	0.000502	0.63	1.601	7.97	7.93	7.85	0.00	0.43	−0.22	1.01
32	0.000459	0.69	1.328	9.90	13.94	13.78	−1.41	−1.00	−0.34	1.15
32	0.000422	0.75	1.406	13.22	40.24	39.94	−4.09	2.17	−0.43	1.45
45	0.003423	0.13	0.935	3.66	3.79	3.59	0.00	−0.65	0.06	1.00
45	0.002023	0.22	1.129	3.99	5.27	5.17	0.00	−0.16	−0.10	1.01
45	0.001435	0.31	1.165	4.74	5.11	5.01	0.00	0.14	0.11	1.00
45	0.001112	0.40	1.328	5.56	5.70	5.60	0.00	0.32	−0.19	1.01
45	0.000927	0.48	1.441	6.40	6.87	6.79	0.00	0.15	−0.21	1.01
45	0.000795	0.56	1.304	7.14	6.62	6.48	0.00	0.80	−0.45	1.00
45	0.000706	0.63	1.444	8.93	8.48	8.38	0.00	0.80	−0.08	1.00
45	0.000645	0.69	1.796	10.82	13.24	13.15	−0.75	−0.84	0.14	1.08
45	0.000593	0.75	1.544	13.35	20.68	20.54	−1.39	1.61	−0.14	1.14
60	0.004564	0.13	0.843	4.51	4.85	4.72	0.00	−0.36	0.25	1.00
60	0.002697	0.22	1.002	4.92	4.90	4.79	0.00	−0.31	−0.00	1.00
60	0.001914	0.31	1.125	5.95	7.10	7.01	−0.44	0.00	−0.14	1.05
60	0.001483	0.40	1.402	6.97	7.61	7.52	−0.24	0.35	−0.10	1.03
60	0.001236	0.48	1.662	7.63	7.62	7.56	0.00	0.00	−0.03	1.01
60	0.001060	0.56	1.445	8.67	8.51	8.43	0.00	0.52	−0.21	1.00
60	0.000942	0.63	2.057	10.98	14.11	14.02	0.00	1.15	−0.22	1.00
60	0.000860	0.69	1.570	12.47	16.00	15.92	−1.13	0.01	−0.18	1.11
60	0.000791	0.75	1.578	17.96	17.26	17.09	0.00	−2.26	0.55	0.62

(Table continued)

TABLE II. (*Continued*)

Q^2 (GeV^2)	x	y	$\tilde{\sigma}$ HER	δ_{stat} (%)	δ_{sys} (%)	δ_{unc} (%)	$\delta_{\gamma p}$ (%)	$\delta_{E_{\text{had}}}$ (%)	δ_{diff} (%)	δ_{hits} (%)
80	0.006085	0.13	0.981	4.86	5.97	5.86	0.00	−0.46	0.19	1.00
80	0.003596	0.22	1.017	5.74	5.94	5.85	0.00	−0.11	−0.03	1.00
80	0.002552	0.31	1.204	6.80	6.70	6.62	0.00	0.00	−0.14	1.00
80	0.001978	0.40	0.972	8.73	7.79	7.72	0.00	0.24	−0.09	1.01
80	0.001648	0.48	1.272	9.43	8.73	8.63	0.00	0.71	−0.35	1.02
80	0.001413	0.56	1.273	10.99	10.40	10.31	−0.34	0.74	−0.33	1.04
80	0.001256	0.63	1.281	14.59	12.61	12.54	0.00	0.94	0.57	0.88
110	0.008367	0.13	0.969	5.80	6.46	6.34	0.00	−0.75	0.06	1.00
110	0.004944	0.22	1.120	6.33	7.05	6.97	0.00	0.32	−0.20	1.00
110	0.003509	0.31	1.194	7.92	8.08	8.02	0.00	−0.23	−0.05	1.00
110	0.002719	0.40	1.073	9.71	8.40	8.34	0.00	0.00	−0.02	1.00
110	0.002266	0.48	1.364	11.40	11.68	11.63	0.00	0.49	−0.30	0.92
110	0.001942	0.56	1.381	17.15	21.36	21.35	0.00	0.00	−0.50	0.44

TABLE III. The reduced cross sections, $\tilde{\sigma}$, for the reaction $e^+p \to e^+X$ at $\sqrt{s} = 251$ GeV for the central-vertex region. Further details are as described in the caption of Table I.

Q^2 (GeV^2)	x	y	$\tilde{\sigma}$ MER	δ_{stat} (%)	δ_{sys} (%)	δ_{unc} (%)	$\delta_{\gamma p}$ (%)	$\delta_{E_{\text{had}}}$ (%)	δ_{diff} (%)	δ_{hits} (%)
7	0.000161	0.69	1.388	12.44	16.85	15.52	−1.64	−5.94	−0.63	2.20
7	0.000148	0.75	1.183	8.53	14.60	13.55	−3.93	−2.81	−0.59	2.44
9	0.000298	0.48	1.441	16.01	15.02	14.87	0.00	0.65	−0.69	1.83
9	0.000255	0.56	1.187	8.38	9.18	8.90	−0.75	−0.69	−0.37	1.97
9	0.000227	0.63	1.397	6.02	5.22	4.77	−0.21	−0.87	−0.51	1.83
9	0.000207	0.69	1.149	5.30	8.94	8.16	−1.96	−2.28	−0.56	1.99
9	0.000190	0.75	1.154	4.82	10.37	9.04	−3.04	−3.51	−0.58	1.96
12	0.000614	0.31	1.051	12.15	11.90	11.74	0.00	−0.28	−0.57	1.86
12	0.000476	0.40	1.087	7.88	6.98	6.71	−0.06	0.12	−0.02	1.90
12	0.000397	0.48	1.317	4.79	4.40	3.97	−0.27	−0.05	−0.25	1.87
12	0.000340	0.56	1.257	3.74	4.05	3.46	−0.51	−0.88	−0.37	1.80
12	0.000302	0.63	1.248	3.73	4.44	3.75	−1.05	−1.18	−0.39	1.72
12	0.000276	0.69	1.319	3.47	5.63	4.83	−1.22	−2.04	−0.40	1.59
12	0.000254	0.75	1.359	3.69	7.36	6.42	−2.07	−2.51	−0.54	1.42
17	0.002076	0.13	0.818	7.78	7.31	6.84	0.00	−1.73	−0.04	1.93
17	0.001227	0.22	1.110	5.27	5.47	5.12	0.00	−0.36	−0.09	1.87
17	0.000870	0.31	1.252	3.77	3.61	3.12	0.00	−0.22	−0.15	1.81
17	0.000675	0.40	1.208	3.18	3.01	2.45	−0.08	−0.09	−0.19	1.74
17	0.000562	0.48	1.264	2.85	2.72	2.01	−0.20	−0.76	−0.21	1.64
17	0.000482	0.56	1.306	2.69	2.83	2.23	−0.53	−0.55	−0.28	1.54
17	0.000428	0.63	1.277	3.18	4.70	3.70	−1.12	−2.23	−0.40	1.43
17	0.000391	0.69	1.208	3.59	4.91	4.06	−1.46	−1.95	−0.39	1.26
17	0.000360	0.75	1.344	3.91	7.10	5.35	−1.91	−4.10	−0.53	1.03
24	0.002930	0.13	0.921	2.40	3.21	2.61	0.00	−0.65	0.00	1.75
24	0.001732	0.22	1.112	2.13	3.06	2.55	0.00	−0.17	−0.04	1.68
24	0.001229	0.31	1.128	2.10	2.41	1.81	−0.03	−0.13	−0.04	1.59
24	0.000952	0.40	1.259	2.08	2.20	1.62	−0.04	−0.10	−0.22	1.47
24	0.000794	0.48	1.287	2.20	2.15	1.64	−0.22	−0.27	−0.16	1.34
24	0.000680	0.56	1.342	2.32	2.32	1.92	−0.31	−0.47	−0.18	1.17
24	0.000605	0.63	1.269	2.98	3.39	2.77	−0.82	−1.44	−0.29	1.01
24	0.000552	0.69	1.371	3.19	3.69	2.77	−0.84	−2.12	−0.29	0.79
24	0.000508	0.75	1.386	3.85	5.67	4.74	−1.93	−2.35	−0.37	0.56
32	0.003907	0.13	0.881	1.70	2.20	1.46	0.00	−0.65	0.06	1.50
32	0.002309	0.22	1.018	1.76	2.37	1.90	0.00	−0.19	0.02	1.40
32	0.001638	0.31	1.132	1.88	1.89	1.38	−0.01	−0.10	−0.11	1.28
32	0.001270	0.40	1.226	2.11	2.17	1.83	−0.07	−0.23	−0.14	1.13

(Table continued)

TABLE III. (*Continued*)

Q^2 (GeV^2)	x	y	$\tilde{\sigma}$ MER	δ_{stat} (%)	δ_{sys} (%)	δ_{unc} (%)	$\delta_{\gamma p}$ (%)	$\delta_{E_{\text{had}}}$ (%)	δ_{diff} (%)	δ_{hits} (%)
32	0.001058	0.48	1.287	2.37	2.01	1.74	−0.13	−0.14	−0.18	0.97
32	0.000907	0.56	1.242	2.68	2.60	2.27	−0.42	−0.87	−0.15	0.79
32	0.000806	0.63	1.316	3.43	3.56	3.36	−0.77	−0.57	−0.33	0.59
32	0.000736	0.69	1.296	3.85	3.72	3.50	−0.92	−0.76	−0.24	0.38
32	0.000677	0.75	1.268	4.57	7.54	5.87	−1.77	−4.38	−0.31	0.21
45	0.005494	0.13	0.905	1.53	2.16	1.70	0.00	−0.61	0.06	1.18
45	0.003247	0.22	1.031	1.71	2.12	1.83	−0.01	−0.10	0.04	1.06
45	0.002304	0.31	1.114	1.96	1.78	1.51	−0.01	−0.18	−0.05	0.92
45	0.001786	0.40	1.165	2.32	1.81	1.63	−0.02	0.10	−0.17	0.76
45	0.001488	0.48	1.211	2.68	2.62	2.53	−0.18	−0.20	−0.15	0.60
45	0.001275	0.56	1.306	2.92	2.30	2.22	−0.26	−0.26	−0.22	0.41
45	0.001134	0.63	1.358	3.76	3.05	2.90	−0.42	−0.76	−0.32	0.25
45	0.001035	0.69	1.426	4.08	3.42	3.20	−0.58	−0.99	−0.28	−0.11
45	0.000952	0.75	1.409	4.65	5.80	5.60	−1.19	−0.90	−0.26	−0.02
60	0.007326	0.13	0.822	1.78	1.84	1.51	0.00	−0.64	0.16	0.82
60	0.004329	0.22	0.974	2.00	2.15	2.01	0.00	−0.26	0.00	0.70
60	0.003072	0.31	1.100	2.29	1.82	1.73	0.00	−0.13	−0.04	0.56
60	0.002381	0.40	1.163	2.72	1.99	1.94	0.00	−0.08	−0.17	0.41
60	0.001984	0.48	1.106	3.30	2.28	2.25	−0.05	0.22	−0.14	0.27
60	0.001701	0.56	1.294	3.51	2.62	2.60	−0.20	0.09	−0.25	0.13
60	0.001512	0.63	1.345	4.41	3.47	3.38	−0.33	−0.71	−0.18	−0.04
60	0.001380	0.69	1.429	4.94	4.09	3.99	−0.69	−0.62	−0.13	−0.01
60	0.001270	0.75	1.436	5.53	5.07	4.76	−0.79	−1.55	−0.15	0.00
80	0.009768	0.13	0.776	2.07	1.82	1.70	0.00	−0.43	0.16	0.48
80	0.005772	0.22	0.953	2.27	2.22	2.18	0.00	−0.09	0.11	0.37
80	0.004096	0.31	1.021	2.70	2.02	2.00	−0.01	0.14	0.03	0.25
80	0.003175	0.40	1.114	3.22	2.54	2.54	−0.01	−0.14	−0.03	0.14
80	0.002645	0.48	1.167	3.65	2.86	2.84	−0.06	0.23	−0.21	−0.06
80	0.002268	0.56	1.172	4.21	3.32	3.29	−0.39	−0.20	−0.07	−0.01
80	0.002016	0.63	1.270	5.28	5.34	5.32	−0.29	−0.35	−0.10	−0.00
80	0.001840	0.69	1.294	5.83	4.44	4.26	−0.57	−1.06	−0.27	0.00
80	0.001693	0.75	1.499	6.14	5.24	5.11	−0.66	−0.97	−0.22	0.00
110	0.013431	0.13	0.702	2.43	2.18	2.10	0.00	−0.54	0.16	0.18
110	0.007936	0.22	0.854	2.74	1.95	1.94	0.00	−0.17	0.09	−0.11
110	0.005632	0.31	0.981	3.15	2.11	2.10	−0.02	−0.14	0.02	−0.04
110	0.004365	0.40	1.066	3.74	2.61	2.61	−0.01	0.12	0.09	−0.01
110	0.003638	0.48	1.163	4.36	2.97	2.96	0.00	−0.12	−0.12	0.00
110	0.003118	0.56	1.152	4.87	3.58	3.53	−0.22	−0.46	−0.27	0.00
110	0.002771	0.63	1.191	6.43	4.67	4.62	−0.37	0.41	−0.29	0.00
110	0.002530	0.69	1.097	7.59	5.95	5.88	−0.37	−0.82	−0.18	0.00

TABLE IV. The reduced cross sections, $\tilde{\sigma}$, for the reaction $e^+p \to e^+X$ at $\sqrt{s} = 251$ GeV for the shifted-vertex region. Further details are as described in the caption of Table I.

Q^2 (GeV^2)	x	y	$\tilde{\sigma}$ MER	δ_{stat} (%)	δ_{sys} (%)	δ_{unc} (%)	$\delta_{\gamma p}$ (%)	$\delta_{E_{\text{had}}}$ (%)	δ_{diff} (%)	δ_{hits} (%)
5	0.000126	0.63	1.189	13.57	13.03	12.97	0.00	−0.37	−0.39	1.09
7	0.000278	0.40	1.123	12.50	13.23	13.19	0.00	−0.63	−0.05	0.74
7	0.000231	0.48	1.173	9.63	9.46	9.40	−0.11	−0.38	0.13	1.00
7	0.000198	0.56	1.229	9.74	14.02	13.93	−0.93	0.54	−0.21	1.12
7	0.000176	0.63	1.225	10.51	12.08	12.01	−0.16	−0.65	−0.35	1.03
7	0.000161	0.69	1.650	11.15	11.36	11.17	−0.38	1.67	−0.36	1.07
7	0.000148	0.75	1.036	15.29	20.39	20.04	−3.19	−1.45	−0.38	1.33
9	0.001099	0.13	0.685	12.88	13.68	13.65	0.00	−0.50	0.00	0.66
9	0.000649	0.22	1.218	7.80	9.61	9.56	0.00	0.14	−0.04	0.89

(Table continued)

TABLE IV. (*Continued*)

Q^2 (GeV^2)	x	y	$\tilde{\sigma}$ MER	δ_{stat} (%)	δ_{sys} (%)	δ_{unc} (%)	$\delta_{\gamma p}$ (%)	$\delta_{E_{\text{had}}}$ (%)	δ_{diff} (%)	δ_{hits} (%)
9	0.000461	0.31	1.107	6.82	7.52	7.45	0.00	0.00	−0.01	1.00
9	0.000357	0.40	1.123	7.28	7.71	7.63	−0.05	−0.23	−0.38	1.02
9	0.000298	0.48	1.220	7.54	6.97	6.88	−0.28	0.26	−0.17	1.04
9	0.000255	0.56	1.194	8.01	8.87	8.80	−0.08	−0.48	−0.13	1.02
9	0.000227	0.63	1.506	9.27	8.12	7.96	−0.12	−1.18	−0.26	1.02
9	0.000207	0.69	1.401	10.23	8.42	8.14	−0.32	−1.83	−0.26	1.05
9	0.000190	0.75	0.995	13.85	13.68	13.51	−1.52	−1.06	−0.12	1.17
12	0.001465	0.13	0.836	5.40	7.29	7.17	0.00	−0.86	0.12	1.01
12	0.000866	0.22	0.979	5.50	6.86	6.78	0.00	0.39	−0.12	1.01
12	0.000614	0.31	1.164	5.77	5.27	5.15	−0.03	0.47	0.02	1.01
12	0.000476	0.40	1.073	7.20	7.23	7.13	−0.40	0.44	0.09	1.05
12	0.000397	0.48	1.149	7.60	6.11	6.02	0.00	−0.41	−0.10	1.01
12	0.000340	0.56	1.330	7.79	7.24	7.14	−0.08	0.60	−0.26	1.02
12	0.000302	0.63	0.743	16.22	31.99	31.63	−3.56	−2.85	−0.43	1.39
12	0.000276	0.69	1.367	11.48	9.41	9.33	−0.39	0.50	−0.09	1.04
12	0.000254	0.75	1.203	12.91	14.27	11.98	−1.17	−7.58	−0.25	1.12
17	0.002076	0.13	0.884	5.33	4.95	4.84	0.00	−0.23	0.08	1.00
17	0.001227	0.22	1.151	5.30	4.44	4.30	0.00	−0.36	−0.15	1.00
17	0.000870	0.31	0.993	6.54	4.80	4.69	0.00	−0.14	−0.18	1.00
17	0.000675	0.40	1.222	6.89	5.97	5.88	−0.05	−0.18	−0.17	1.01
17	0.000562	0.48	1.238	8.04	7.08	6.98	−0.15	0.63	−0.06	1.03
17	0.000482	0.56	1.175	8.74	7.32	7.23	0.00	−0.26	−0.48	1.01
17	0.000428	0.63	1.331	12.02	9.87	9.74	−0.41	−1.04	−0.42	1.05
17	0.000391	0.69	1.150	13.57	10.96	10.85	−0.94	−0.54	−0.22	1.09
17	0.000360	0.75	1.563	14.57	14.14	14.01	−1.28	−0.78	−0.38	1.13
24	0.002930	0.13	0.980	4.72	4.60	4.35	0.00	−1.06	0.18	1.00
24	0.001732	0.22	0.872	5.77	4.24	4.11	−0.02	0.10	−0.13	1.01
24	0.001229	0.31	1.178	6.12	4.95	4.84	0.00	0.08	−0.02	1.00
24	0.000952	0.40	1.247	7.10	6.54	6.44	0.00	0.35	−0.23	1.01
24	0.000794	0.48	1.215	8.90	9.42	9.28	−0.97	−0.53	−0.24	1.11
24	0.000680	0.56	1.428	9.22	9.54	9.43	−0.21	−1.07	−0.03	1.03
24	0.000605	0.63	1.357	13.03	12.05	11.96	−0.80	0.59	−0.15	1.08
24	0.000552	0.69	1.491	12.90	11.69	11.63	0.00	−0.35	−0.31	1.01
24	0.000508	0.75	1.683	14.09	12.60	12.42	−0.34	−1.72	−0.44	1.04
32	0.003907	0.13	0.907	5.60	4.71	4.55	0.00	−0.71	0.10	1.00
32	0.002309	0.22	0.979	6.54	5.62	5.53	0.00	−0.00	0.14	1.00
32	0.001638	0.31	1.217	7.15	5.64	5.55	0.00	−0.22	0.14	1.00
32	0.001270	0.40	1.497	8.03	6.26	6.18	0.00	0.15	−0.08	1.01
32	0.001058	0.48	1.088	11.17	7.59	7.51	−0.14	−0.15	−0.33	1.02
32	0.000907	0.56	1.251	11.65	9.24	8.91	−0.38	−2.15	−0.46	1.04
32	0.000806	0.63	1.702	13.24	10.56	10.48	0.00	0.81	−0.00	1.01
32	0.000736	0.69	1.256	16.03	11.86	11.75	−0.74	−0.79	−0.19	1.08
32	0.000677	0.75	1.415	19.40	15.37	15.28	−1.12	−0.62	0.02	1.11
45	0.005494	0.13	0.825	6.67	5.55	5.43	0.00	−0.43	0.34	1.00
45	0.003247	0.22	0.817	7.86	5.52	5.43	0.00	−0.11	−0.03	1.00
45	0.002304	0.31	1.179	8.68	6.53	6.45	0.00	0.31	0.10	1.01
45	0.001786	0.40	1.250	9.95	8.48	8.40	0.00	0.46	−0.07	1.01
45	0.001488	0.48	1.278	11.38	8.94	8.86	0.00	−0.49	−0.27	1.01
45	0.001275	0.56	0.985	15.16	11.62	11.53	0.00	−1.07	0.04	1.01
45	0.001134	0.63	1.224	18.27	14.98	14.93	0.00	0.57	−0.44	1.00
45	0.001035	0.69	1.057	19.17	11.42	11.33	0.00	0.70	−0.72	1.01
60	0.007326	0.13	0.757	8.26	5.87	5.72	0.00	−0.84	0.15	1.00
60	0.004329	0.22	0.865	9.15	6.65	6.56	0.00	−0.15	0.26	1.00
60	0.003072	0.31	0.988	10.79	7.04	6.96	0.00	0.41	0.04	1.01
60	0.002381	0.40	1.522	11.40	9.82	9.72	0.00	−0.96	−0.10	1.01
60	0.001984	0.48	1.525	12.89	10.05	9.98	0.00	−0.40	−0.65	1.01

(Table continued)

TABLE IV. (*Continued*)

Q^2 (GeV^2)	x	y	$\tilde{\sigma}$ MER	δ_{stat} (%)	δ_{sys} (%)	δ_{unc} (%)	$\delta_{\gamma p}$ (%)	$\delta_{E_{\text{had}}}$ (%)	δ_{diff} (%)	δ_{hits} (%)
60	0.001701	0.56	1.342	15.74	10.89	10.82	0.00	0.48	−0.41	1.02
60	0.001512	0.63	1.276	20.03	55.38	55.37	0.00	0.98	0.16	1.00
80	0.009768	0.13	0.674	9.72	7.14	7.07	0.00	0.16	−0.05	1.00
80	0.005772	0.22	1.009	9.92	7.67	7.59	0.00	0.41	−0.14	1.00
80	0.004096	0.31	1.159	12.17	9.56	9.49	0.00	−0.62	0.03	1.00
80	0.003175	0.40	1.218	13.69	10.36	10.31	0.00	0.03	−0.04	1.01
80	0.002645	0.48	1.276	17.62	17.22	17.13	−0.81	−1.17	−0.17	1.09
80	0.002268	0.56	0.907	22.78	21.80	21.71	−1.34	0.73	0.02	1.14
110	0.013431	0.13	0.710	11.63	8.30	8.21	0.00	0.49	0.40	1.00
110	0.007936	0.22	0.780	13.18	9.39	9.33	0.00	0.01	0.24	1.00
110	0.005632	0.31	0.932	14.68	10.20	10.08	0.00	1.15	−0.30	1.01
110	0.004365	0.40	1.132	17.06	11.86	11.80	0.00	0.58	−0.30	1.01

TABLE V. The reduced cross sections, $\tilde{\sigma}$, for the reaction $e^+p \to e^+X$ at $\sqrt{s} = 225$ GeV for the central-vertex region. Further details are as described in the caption of Table I.

Q^2 (GeV^2)	x	y	$\tilde{\sigma}$ LER	δ_{stat} (%)	δ_{sys} (%)	δ_{unc} (%)	$\delta_{\gamma p}$ (%)	$\delta_{E_{\text{had}}}$ (%)	δ_{diff} (%)	δ_{hits} (%)
7	0.000219	0.63	1.543	14.72	12.67	12.43	−0.63	−1.12	−0.80	1.92
7	0.000200	0.69	1.204	9.26	9.98	9.34	−1.51	−2.24	−0.70	2.14
7	0.000184	0.75	1.332	5.72	8.80	7.20	−2.26	−3.93	−0.69	2.14
9	0.000370	0.48	1.259	11.80	8.72	8.50	−0.28	−0.16	−0.35	1.89
9	0.000317	0.56	1.053	7.02	6.48	6.14	−0.27	−0.64	−0.28	1.93
9	0.000282	0.63	1.294	4.58	4.44	3.57	−0.41	−1.77	−0.42	1.87
9	0.000258	0.69	1.312	3.73	6.03	4.70	−1.90	−2.50	−0.58	2.00
9	0.000237	0.75	1.318	3.22	6.47	4.55	−2.13	−3.58	−0.65	1.82
12	0.001077	0.22	0.781	16.48	11.13	11.00	0.00	0.00	0.06	1.72
12	0.000765	0.31	1.219	8.12	6.18	5.88	−0.10	−0.15	−0.15	1.89
12	0.000593	0.40	1.158	5.20	3.98	3.50	0.00	−0.14	−0.14	1.88
12	0.000494	0.48	1.214	3.64	3.41	2.82	−0.26	−0.32	−0.20	1.85
12	0.000423	0.56	1.299	2.66	3.23	2.53	−0.52	−0.62	−0.40	1.79
12	0.000376	0.63	1.278	2.71	4.11	3.33	−0.89	−1.36	−0.45	1.72
12	0.000344	0.69	1.219	2.72	4.80	3.70	−1.59	−1.95	−0.52	1.64
12	0.000316	0.75	1.357	2.74	6.03	3.86	−1.98	−3.88	−0.58	1.44
17	0.002583	0.13	0.829	5.55	4.40	3.90	0.00	−0.73	0.13	1.91
17	0.001526	0.22	1.035	3.84	4.04	3.57	0.00	−0.15	0.02	1.87
17	0.001083	0.31	1.191	2.85	2.78	2.09	−0.07	−0.18	−0.09	1.82
17	0.000840	0.40	1.218	2.35	2.41	1.65	−0.05	−0.19	−0.18	1.73
17	0.000700	0.48	1.225	2.14	2.16	1.30	−0.18	−0.40	−0.25	1.64
17	0.000600	0.56	1.303	1.96	2.22	1.41	−0.44	−0.58	−0.30	1.53
17	0.000533	0.63	1.253	2.35	3.06	2.33	−0.79	−1.12	−0.32	1.40
17	0.000487	0.69	1.274	2.51	3.38	2.34	−1.10	−1.75	−0.42	1.22
17	0.000448	0.75	1.255	2.95	4.79	3.29	−2.03	−2.59	−0.45	1.04
24	0.003647	0.13	0.887	1.80	2.71	1.95	0.00	−0.69	0.07	1.74
24	0.002155	0.22	1.043	1.61	2.49	1.84	−0.00	−0.19	−0.06	1.68
24	0.001529	0.31	1.094	1.56	2.03	1.26	−0.03	−0.11	−0.08	1.59
24	0.001185	0.40	1.161	1.59	1.83	1.06	−0.09	−0.14	−0.18	1.48
24	0.000988	0.48	1.201	1.66	1.92	1.29	−0.18	−0.38	−0.21	1.35
24	0.000847	0.56	1.269	1.71	2.09	1.59	−0.35	−0.53	−0.25	1.18
24	0.000752	0.63	1.264	2.18	2.46	1.78	−0.68	−1.15	−0.30	1.01
24	0.000687	0.69	1.280	2.46	2.91	2.27	−1.06	−1.19	−0.33	0.82
24	0.000632	0.75	1.273	2.82	4.72	3.05	−1.83	−3.03	−0.35	0.56
32	0.004862	0.13	0.859	1.27	2.31	1.65	−0.00	−0.58	0.08	1.50
32	0.002873	0.22	0.990	1.31	2.24	1.74	−0.00	−0.19	0.01	1.40
32	0.002039	0.31	1.077	1.42	1.53	0.83	−0.01	−0.11	−0.11	1.28

(Table continued)

TABLE V. (*Continued*)

Q^2 (GeV^2)	x	y	$\tilde{\sigma}$ LER	δ_{stat} (%)	δ_{sys} (%)	δ_{unc} (%)	$\delta_{\gamma p}$ (%)	$\delta_{E_{\text{had}}}$ (%)	δ_{diff} (%)	δ_{hits} (%)
32	0.001580	0.40	1.168	1.57	1.70	1.24	−0.06	−0.20	−0.15	1.13
32	0.001317	0.48	1.258	1.75	1.52	1.11	−0.16	−0.22	−0.18	0.98
32	0.001129	0.56	1.248	1.97	1.76	1.45	−0.35	−0.47	−0.18	0.79
32	0.001003	0.63	1.275	2.55	2.14	1.76	−0.60	−0.83	−0.20	0.60
32	0.000916	0.69	1.398	2.67	2.45	1.95	−0.61	−1.27	−0.26	0.39
32	0.000843	0.75	1.292	3.24	4.21	2.77	−1.47	−2.79	−0.27	0.20
45	0.006838	0.13	0.823	1.18	1.90	1.34	0.00	−0.65	0.10	1.18
45	0.004040	0.22	0.944	1.30	2.06	1.75	0.00	−0.14	0.00	1.06
45	0.002867	0.31	1.098	1.45	1.31	0.92	−0.01	−0.12	−0.09	0.93
45	0.002222	0.40	1.109	1.74	1.30	1.03	−0.06	−0.10	−0.11	0.77
45	0.001852	0.48	1.119	2.02	1.46	1.30	−0.11	−0.21	−0.14	0.60
45	0.001587	0.56	1.255	2.18	1.60	1.39	−0.16	−0.60	−0.23	0.42
45	0.001411	0.63	1.228	2.83	1.93	1.69	−0.42	−0.78	−0.19	0.25
45	0.001288	0.69	1.284	3.15	2.68	2.33	−0.74	−1.07	−0.20	−0.11
45	0.001185	0.75	1.260	3.51	4.10	3.63	−1.00	−1.61	−0.24	−0.03
60	0.009117	0.13	0.761	1.35	1.61	1.23	0.00	−0.58	0.16	0.83
60	0.005387	0.22	0.897	1.53	1.81	1.66	0.00	−0.14	0.01	0.71
60	0.003823	0.31	1.009	1.75	1.20	1.06	−0.01	−0.04	−0.07	0.57
60	0.002963	0.40	1.107	2.04	1.40	1.33	−0.02	−0.10	−0.13	0.42
60	0.002469	0.48	1.153	2.34	1.62	1.57	−0.11	−0.17	−0.15	0.28
60	0.002116	0.56	1.198	2.65	1.73	1.70	−0.17	−0.20	−0.16	0.13
60	0.001881	0.63	1.198	3.46	3.24	3.12	−0.59	−0.58	−0.16	−0.05
60	0.001718	0.69	1.251	3.73	2.92	2.73	−0.78	−0.68	−0.21	−0.01
60	0.001580	0.75	1.213	4.27	3.66	3.40	−1.11	−0.80	−0.15	0.00
80	0.012156	0.13	0.726	1.55	1.52	1.32	0.00	−0.58	0.11	0.48
80	0.007183	0.22	0.917	1.69	1.61	1.56	0.00	−0.13	0.05	0.37
80	0.005098	0.31	0.961	2.02	1.13	1.10	−0.01	−0.09	−0.04	0.26
80	0.003951	0.40	1.043	2.38	1.31	1.30	−0.03	0.04	−0.04	0.15
80	0.003292	0.48	1.110	2.74	1.39	1.37	−0.01	−0.17	−0.12	−0.06
80	0.002822	0.56	1.124	3.09	2.19	2.17	−0.15	0.19	−0.11	−0.01
80	0.002508	0.63	1.172	3.95	2.75	2.70	−0.40	0.24	−0.17	0.00
80	0.002290	0.69	1.095	4.51	3.29	3.22	−0.56	−0.16	−0.26	0.00
80	0.002107	0.75	1.285	4.75	3.80	3.57	−0.81	−0.99	−0.33	0.00
110	0.016714	0.13	0.679	1.80	1.75	1.62	0.00	−0.62	0.15	0.19
110	0.009877	0.22	0.822	2.04	1.51	1.50	0.00	−0.08	0.10	−0.11
110	0.007009	0.31	0.890	2.42	1.18	1.18	−0.01	0.11	0.03	−0.05
110	0.005432	0.40	0.994	2.80	1.51	1.51	0.00	−0.07	−0.03	−0.01
110	0.004527	0.48	1.117	3.19	1.73	1.71	−0.10	−0.15	−0.13	0.00
110	0.003880	0.56	1.050	3.69	1.85	1.84	−0.07	−0.06	−0.15	0.00
110	0.003449	0.63	1.199	4.68	3.84	3.81	−0.31	−0.33	−0.16	0.00
110	0.003149	0.69	1.209	5.27	3.34	3.23	−0.38	−0.72	−0.29	0.00
110	0.002897	0.75	0.940	9.18	6.18	6.10	−0.94	−0.17	−0.31	0.00

TABLE VI. The reduced cross sections, $\tilde{\sigma}$, for the reaction $e^+p \to e^+X$ at $\sqrt{s} = 225$ GeV for the shifted-vertex region. Further details are as described in the caption of Table I.

Q^2 (GeV^2)	x	y	$\tilde{\sigma}$ LER	δ_{stat} (%)	δ_{sys} (%)	δ_{unc} (%)	$\delta_{\gamma p}$ (%)	$\delta_{E_{\text{had}}}$ (%)	δ_{diff} (%)	δ_{hits} (%)
5	0.000176	0.56	1.022	10.84	7.82	7.74	−0.28	−0.54	−0.37	0.90
5	0.000157	0.63	1.011	10.04	9.90	9.76	−0.27	−1.09	−0.34	1.10
5	0.000143	0.69	1.049	10.23	9.43	9.23	−1.02	−1.05	−0.54	1.18
7	0.000446	0.31	0.952	15.23	10.10	10.08	0.00	0.43	−0.26	0.35
7	0.000346	0.40	0.964	9.54	6.63	6.57	0.00	0.33	−0.07	0.83
7	0.000288	0.48	0.870	7.67	6.58	6.49	−0.18	−0.18	−0.21	1.03
7	0.000247	0.56	1.074	6.84	7.66	7.39	−0.63	−1.56	−0.24	1.08

(Table continued)

TABLE VI. (*Continued*)

Q^2 (GeV^2)	x	y	$\tilde{\sigma}$ LER	δ_{stat} (%)	δ_{sys} (%)	δ_{unc} (%)	$\delta_{\gamma p}$ (%)	$\delta_{E_{\text{had}}}$ (%)	δ_{diff} (%)	δ_{hits} (%)
7	0.000219	0.63	1.114	7.79	7.90	7.73	−0.39	−1.14	−0.21	1.06
7	0.000200	0.69	1.075	9.14	14.24	11.69	−2.08	−7.75	−0.38	1.22
7	0.000184	0.75	1.334	9.00	11.40	11.11	−1.64	−1.51	−0.41	1.18
9	0.001368	0.13	0.874	7.77	6.49	6.38	0.00	−0.96	0.15	0.67
9	0.000808	0.22	0.940	5.96	5.58	5.50	−0.02	−0.21	0.03	0.91
9	0.000573	0.31	1.040	4.99	5.14	5.04	0.00	0.11	0.01	1.00
9	0.000444	0.40	1.130	4.96	5.81	5.71	−0.09	−0.30	−0.17	1.02
9	0.000370	0.48	0.990	5.78	5.28	5.11	−0.67	−0.41	−0.11	1.08
9	0.000317	0.56	1.282	5.28	4.79	4.66	−0.30	0.09	−0.22	1.03
9	0.000282	0.63	1.063	7.22	5.64	5.47	−0.52	−0.51	−0.49	1.07
9	0.000258	0.69	1.211	7.75	7.06	6.62	−0.91	−1.97	−0.36	1.10
9	0.000237	0.75	0.703	13.78	23.78	22.87	−6.15	−1.34	−0.51	1.65
12	0.001823	0.13	0.812	3.86	4.46	4.29	0.00	−0.64	0.10	1.00
12	0.001077	0.22	1.017	3.74	4.53	4.42	0.00	−0.13	0.01	1.01
12	0.000765	0.31	0.966	4.34	3.78	3.63	−0.01	−0.31	0.00	1.01
12	0.000593	0.40	1.106	4.68	3.80	3.66	−0.04	−0.08	−0.08	1.01
12	0.000494	0.48	1.067	5.47	4.82	4.67	−0.43	−0.17	−0.23	1.05
12	0.000423	0.56	1.138	5.65	4.79	4.65	−0.14	−0.44	−0.20	1.02
12	0.000376	0.63	0.926	8.40	7.00	6.84	−0.95	−0.41	−0.17	1.10
12	0.000344	0.69	1.319	8.21	7.20	7.00	−1.09	−0.60	−0.15	1.12
12	0.000316	0.75	1.275	9.10	7.45	7.11	−1.12	−1.49	−0.40	1.12
17	0.002583	0.13	0.813	3.72	3.94	3.72	0.00	−0.84	0.09	1.00
17	0.001526	0.22	0.901	4.04	3.75	3.60	0.00	−0.30	−0.08	1.01
17	0.001083	0.31	1.137	4.18	3.68	3.53	0.00	−0.11	−0.02	1.01
17	0.000840	0.40	1.108	5.00	4.00	3.87	−0.02	−0.14	−0.15	1.01
17	0.000700	0.48	1.034	6.05	5.06	4.93	−0.40	−0.17	−0.13	1.05
17	0.000600	0.56	1.257	6.07	4.58	4.46	−0.14	0.14	−0.08	1.02
17	0.000533	0.63	1.240	8.48	5.99	5.83	−0.47	0.64	−0.23	1.05
17	0.000487	0.69	1.076	10.76	12.02	11.56	−2.20	−2.07	−0.23	1.23
17	0.000448	0.75	1.259	10.72	8.14	7.96	−0.83	−0.97	−0.24	1.09
24	0.003647	0.13	0.834	3.46	3.63	3.43	0.00	−0.60	0.22	1.00
24	0.002155	0.22	0.928	3.80	3.56	3.41	0.00	−0.16	−0.02	1.00
24	0.001529	0.31	1.030	4.38	3.30	3.14	0.00	−0.23	−0.03	1.01
24	0.001185	0.40	1.230	4.83	3.68	3.52	0.00	−0.25	−0.12	1.01
24	0.000988	0.48	1.125	5.90	3.96	3.82	−0.03	−0.05	−0.30	1.01
24	0.000847	0.56	1.129	7.08	5.23	5.11	−0.28	−0.23	−0.17	1.03
24	0.000752	0.63	0.979	9.91	7.61	7.47	−0.86	−0.25	−0.26	1.10
24	0.000687	0.69	1.391	9.02	6.25	6.08	−0.82	−0.38	−0.17	1.09
24	0.000632	0.75	1.274	10.03	6.32	6.17	−0.28	−0.78	−0.34	1.03
32	0.004862	0.13	0.815	4.02	3.69	3.47	0.00	−0.72	0.08	1.00
32	0.002873	0.22	0.998	4.29	3.85	3.72	0.00	−0.09	−0.07	1.00
32	0.002039	0.31	0.982	5.32	3.49	3.34	0.00	0.12	−0.04	1.01
32	0.001580	0.40	1.152	6.07	3.94	3.80	−0.03	0.03	−0.19	1.01
32	0.001317	0.48	0.991	7.94	6.62	6.50	−0.59	0.24	−0.19	1.07
32	0.001129	0.56	1.073	8.55	5.26	5.15	−0.17	0.07	−0.07	1.02
32	0.001003	0.63	1.028	11.08	5.88	5.77	−0.28	−0.46	−0.18	1.03
32	0.000916	0.69	1.257	11.42	6.47	6.36	−0.16	0.03	−0.54	1.02
32	0.000843	0.75	1.692	11.29	8.11	8.02	−0.42	0.22	−0.23	1.05
45	0.006838	0.13	0.796	4.54	4.03	3.84	0.00	−0.69	0.12	1.00
45	0.004040	0.22	0.885	5.25	3.89	3.76	−0.04	0.09	−0.07	1.01
45	0.002867	0.31	0.984	6.08	3.98	3.85	0.00	0.08	−0.11	1.01
45	0.002222	0.40	1.020	7.32	4.49	4.37	0.00	−0.10	−0.22	1.01
45	0.001852	0.48	1.161	8.25	4.94	4.82	0.00	0.13	−0.34	1.01
45	0.001587	0.56	1.405	8.57	5.22	5.11	0.00	−0.23	−0.10	1.01
45	0.001411	0.63	1.513	10.73	7.40	7.32	−0.13	0.23	−0.17	1.02
45	0.001288	0.69	1.530	13.06	10.24	9.92	−1.08	−1.97	−0.45	1.11

(Table continued)

TABLE VI. (*Continued*)

Q^2 (GeV^2)	x	y	$\tilde{\sigma}$ LER	δ_{stat} (%)	δ_{sys} (%)	δ_{unc} (%)	$\delta_{\gamma p}$ (%)	$\delta_{E_{\text{had}}}$ (%)	δ_{diff} (%)	δ_{hits} (%)
45	0.001185	0.75	1.033	17.90	15.83	15.63	−2.13	0.38	−0.27	1.21
60	0.009117	0.13	0.708	5.71	3.80	3.58	0.00	−0.76	0.18	1.00
60	0.005387	0.22	0.846	6.30	4.25	4.12	0.00	−0.29	−0.02	1.00
60	0.003823	0.31	1.013	7.24	4.32	4.19	0.00	0.27	−0.05	1.01
60	0.002963	0.40	1.011	8.60	4.96	4.85	0.00	0.24	−0.02	1.01
60	0.002469	0.48	1.069	10.47	6.06	5.98	0.00	−0.13	0.07	1.00
60	0.002116	0.56	1.292	11.12	5.86	5.75	0.00	0.47	0.06	1.01
60	0.001881	0.63	0.948	18.67	25.30	25.16	−2.27	0.40	−0.15	1.24
60	0.001718	0.69	1.531	15.44	9.43	9.36	0.00	0.53	−0.39	0.98
80	0.012156	0.13	0.706	6.48	4.22	4.03	0.00	−0.68	0.15	1.00
80	0.007183	0.22	0.885	7.16	4.41	4.26	0.00	−0.57	−0.11	1.00
80	0.005098	0.31	0.879	8.60	5.12	5.02	0.00	−0.24	−0.03	1.00
80	0.003951	0.40	0.948	10.80	5.42	5.32	0.00	0.29	−0.08	1.01
80	0.003292	0.48	1.058	11.86	5.91	5.79	0.00	0.63	−0.19	1.01
80	0.002822	0.56	0.735	15.48	6.52	6.36	0.00	0.98	−0.04	1.00
80	0.002508	0.63	0.871	21.91	9.78	9.68	0.00	1.05	−0.43	0.80
110	0.016714	0.13	0.619	8.34	4.82	4.65	0.00	−0.73	0.30	1.00
110	0.009877	0.22	0.872	8.60	5.29	5.19	0.00	0.00	0.13	1.01
110	0.007009	0.31	0.960	9.76	5.19	5.09	0.00	0.01	0.04	1.00
110	0.005432	0.40	1.016	11.45	6.37	6.28	0.00	0.23	−0.16	1.00
110	0.004527	0.48	0.960	15.50	8.25	8.15	0.00	0.86	−0.22	0.91

TABLE VII. The reduced cross sections, $\tilde{\sigma}$, for the reaction $e^+p \to e^+X$, at $\sqrt{s} = 300$ GeV measured in the years 1996 and 1997, after the adjustments of the binning for the F_L extraction. The first two columns contain the bin centers in Q^2 and x, the next three contain the measured cross section, the statistical uncertainty and the uncorrelated systematic uncertainty, respectively. The final ten columns list the bin-to-bin correlated uncertainties from each systematic source. The normalization uncertainty (see Sec. VIII) is not included.

Q^2 (GeV^2)	x	y	$\tilde{\sigma}$ ZEUS97	$\tilde{\delta}_{\text{stat}}$ (%)	$\tilde{\delta}_{\text{unc}}$ (%)	$\tilde{\delta}_{\text{eID}}$ (%)	$\tilde{\delta}_{\text{dxdy}}$ (%)	$\tilde{\delta}_{e\theta}$ (%)	$\tilde{\delta}_{E_e}$ (%)	$\tilde{\delta}_{\text{hdFC}}$ (%)	$\tilde{\delta}_{\text{hdBC}}$ (%)	$\tilde{\delta}_{\text{hdRC}}$ (%)	$\tilde{\delta}_{\text{hdF}}$ (%)	$\tilde{\delta}_{\text{Bhd}}$ (%)	$\tilde{\delta}_{\gamma p}$ (%)
9	0.00025	0.40	1.214	1.60	0.90	1.64	0.56	0.00	0.59	−0.08	0.21	0.39	0.24	1.61	0.20
9	0.00040	0.25	1.086	1.64	0.92	1.38	0.59	0.00	−0.44	0.08	0.18	−0.36	0.10	0.63	−0.18
12	0.00033	0.40	1.270	2.61	0.96	2.21	1.26	0.00	−0.95	0.22	0.29	0.98	0.54	6.78	0.24
12	0.00041	0.33	1.186	2.30	0.87	1.61	0.59	0.00	0.22	−0.16	−0.06	0.13	0.26	1.87	−0.01
12	0.00054	0.25	1.106	2.30	0.87	1.61	0.59	0.00	0.22	−0.16	−0.06	0.13	0.26	1.87	−0.01
17	0.00047	0.40	1.277	1.94	0.68	1.94	0.42	0.00	−0.49	0.11	0.26	0.39	0.22	3.49	0.09
17	0.00076	0.25	1.150	1.94	0.68	1.94	0.42	0.00	−0.49	0.11	0.26	0.39	0.22	3.49	0.09
24	0.00067	0.40	1.315	2.55	1.22	1.99	0.47	0.00	−1.02	0.13	0.23	0.59	0.66	2.83	−0.01
24	0.00082	0.33	1.289	2.20	0.65	1.54	−0.12	0.00	0.27	−0.09	0.35	−0.10	0.25	0.63	−0.49
24	0.00108	0.25	1.140	2.26	1.40	1.30	0.99	0.00	−0.15	−0.17	0.39	−0.55	0.01	0.18	0.12
32	0.00089	0.40	1.351	1.48	0.66	1.89	0.36	0.01	−0.95	−0.02	0.04	0.32	1.05	1.44	−0.01
32	0.00109	0.33	1.253	1.36	0.33	1.49	0.47	0.00	−0.28	−0.07	0.43	−0.46	0.28	0.29	0.05
32	0.00143	0.25	1.199	1.63	0.43	1.29	0.55	0.00	−0.47	−0.15	0.32	−0.36	0.14	0.03	−0.07
45	0.00125	0.40	1.309	1.34	0.34	1.62	0.46	0.00	−0.73	0.03	0.34	−0.78	0.17	0.45	−0.01
45	0.00153	0.33	1.143	1.70	0.39	1.37	0.49	0.00	−0.20	0.09	0.56	−0.27	−0.12	0.15	0.09
60	0.00167	0.40	1.313	1.31	0.55	1.80	0.53	−0.11	−0.44	0.12	0.14	−0.06	0.42	0.72	−0.02
60	0.00204	0.33	1.222	1.49	0.46	1.48	0.38	0.00	−0.23	−0.16	0.35	−0.45	0.42	0.36	−0.14
60	0.00269	0.25	1.129	1.49	0.40	1.31	0.35	0.00	0.16	−0.07	0.36	−0.27	−0.17	0.08	−0.14
80	0.00222	0.40	1.200	1.98	0.35	1.81	0.20	−0.38	−0.83	−0.03	0.36	−0.23	0.23	0.47	0.03
80	0.00272	0.33	1.201	1.85	0.22	1.52	0.43	−0.35	0.26	0.08	0.41	−0.20	−0.06	0.05	0.06
80	0.00359	0.25	1.116	1.68	0.56	1.32	0.15	−0.06	−0.74	−0.09	0.13	−0.17	−0.27	0.00	−0.30
110	0.00306	0.40	1.176	1.93	0.73	1.67	0.30	0.05	−0.69	−0.04	0.31	−0.41	0.02	0.10	−0.03
110	0.00493	0.25	1.030	1.72	0.50	1.41	0.54	−0.71	0.09	−0.16	0.37	−0.22	−0.16	0.08	0.04

VIII. THE ZEUS97 DATA SET

In order to increase the precision of the F_L and F_2 extractions, the reduced NC cross sections measured by ZEUS from the e^+p data taken in 1996 and 1997 with the proton beam energy $E_p = 820$ GeV [19] were included in the analysis. The precision of these data is comparable to the HER data presented in this paper. The binning for the ZEUS97 sample is similar but not identical to that used for the present measurement, so a binning correction was applied to the cross sections from the ZEUS97 sample, using the procedure introduced in an earlier publication [1]. An interpolation of a measurement to the required point on the (x, Q^2) grid is performed by multiplying the measured cross section by the ratio of predicted double-differential cross sections at two different (x, Q^2) points. For the theory calculation, the HERAPDF1.0 next-to-leading-order (NLO) prediction [1] was used. The points required typical adjustments of 0.5%–2%, with a couple of points requiring a 5% adjustment.

The following systematic uncertainties [19] on the cross sections were included in the extraction of F_2 and F_L:

(i) $\{\tilde{\delta}_{\mathrm{eID}}\}$, the uncertainty in the positron-finding efficiency;
(ii) $\{\tilde{\delta}_{\mathrm{dxdy}}\}$, the uncertainty in the positron position;
(iii) $\{\tilde{\delta}_{e\theta}\}$, the uncertainty in the positron-scattering angle;

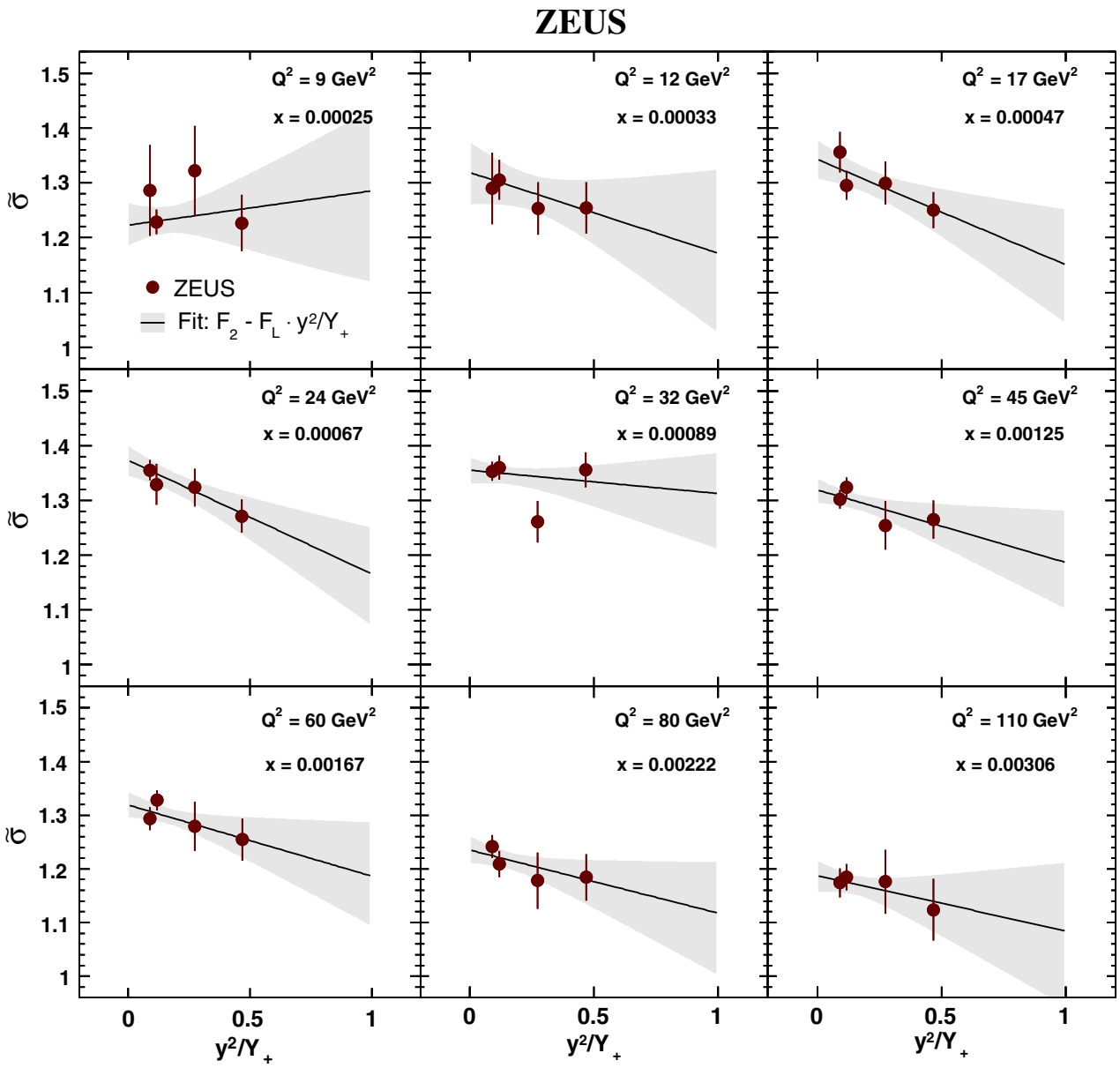

FIG. 7 (color online). Rosenbluth plots for the lowest-x points for each of the 9 Q^2 values for which F_L was measured. The reduced cross sections are shown as points, with error bars representing the combined statistical and systematic uncertainties. The line represents the result from the fit to the reduced cross sections (see Sec. IX), shown together with the 68% uncertainty band.

(iv) $\{\tilde{\delta}_{E_e}\}$, the uncertainty in the positron-energy scale;
(v) $\{\tilde{\delta}_{\mathrm{hdFC}}\}$, $\{\tilde{\delta}_{\mathrm{hdBC}}\}$, $\{\tilde{\delta}_{\mathrm{hdRC}}\}$, the uncertainty in the hadronic-energy scales in FCAL, BCAL and RCAL;
(vi) $\{\tilde{\delta}_{\mathrm{hdF}}\}$, $\{\tilde{\delta}_{\mathrm{Bhd}}\}$, the uncertainty in the hadronic-energy flow;
(vii) $\{\tilde{\delta}_{\gamma p}\}$, the uncertainty in the photoproduction background.

Following the prescription in the publication [19], all uncertainties were treated as correlated.

The fractional systematic uncertainties after the cross-section adjustment were kept unchanged. In addition to the uncertainties mentioned above, the ZEUS97 cross sections have a 2% normalization uncertainty, which resulted from a 1.5% luminosity uncertainty, a 1% trigger uncertainty, a 1% uncertainty from the vertex distribution and a 0.5% uncertainty due to radiative corrections.

The reduced cross sections after the adjustment are given double differentially in bins of x and Q^2 in Table VII.

IX. EXTRACTION OF F_2, F_L AND R

A. Fit method

The values of F_L, F_2 and $R = F_L/(F_2 - F_L)$ were extracted by performing a fit to the reduced cross sections using Eq. (1). The fit was performed with the BAT package [51]. Prior to fitting, the HER, MER and LER cross sections were normalized to ZEUS97 data at low y. This resulted in the following normalization factors for the central- and shifted-vertex samples: $c_{\mathrm{HER,cen}} = 1.025 \pm 0.003$; $c_{\mathrm{MER,cen}} = 1.004 \pm 0.007$; $c_{\mathrm{LER,cen}} = 0.998 \pm 0.004$; $c_{\mathrm{HER,sh}} = 1.042 \pm 0.012$; $c_{\mathrm{MER,sh}} = 1.056 \pm 0.020$; and $c_{\mathrm{LER,sh}} = 1.039 \pm 0.013$. Within the assigned global normalization uncertainties of the respective data sets these numbers are consistent with unity. A different cross-section binning was used for the structure-function extraction in order to cover similar Q^2 and x ranges in each data set, resulting in 27 (x, Q^2) bins. After normalization, the reduced cross sections from the central- and shifted-vertex regions were combined using a weighted average based on their

TABLE VIII. Extracted values of F_2 and F_L at 27 (x, Q^2) points. Values are quoted for the unconstrained and constrained fits. The quoted uncertainties cover both the statistical and systematic sources. The normalization uncertainty (see Sec. IX A) is not included. For the constrained fits with mode at $F_L = 0$, the upper uncertainties correspond to 68% probability limits.

Q^2 (GeV^2)	x	F_2 (unconstrained fit)	F_2 (constrained fit)	F_L (unconstrained fit)	F_L (constrained fit)
9	0.00025	$1.223^{+0.045}_{-0.039}$	$1.259^{+0.039}_{-0.033}$	$-0.06^{+0.22}_{-0.19}$	$0.00^{+0.24}_{-0.00}$
9	0.00031	$1.325^{+0.111}_{-0.129}$	$1.331^{+0.111}_{-0.081}$	$0.25^{+0.55}_{-0.42}$	$0.47^{+0.29}_{-0.41}$
9	0.00040	$1.085^{+0.039}_{-0.033}$	$1.115^{+0.033}_{-0.027}$	$-0.08^{+0.53}_{-0.51}$	$0.00^{+0.57}_{-0.00}$
12	0.00033	$1.319^{+0.063}_{-0.057}$	$1.349^{+0.063}_{-0.051}$	$0.15^{+0.20}_{-0.20}$	$0.29^{+0.20}_{-0.16}$
12	0.00041	$1.181^{+0.045}_{-0.039}$	$1.229^{+0.039}_{-0.027}$	$-0.24^{+0.26}_{-0.20}$	$0.00^{+0.17}_{-0.00}$
12	0.00054	$1.139^{+0.045}_{-0.039}$	$1.169^{+0.033}_{-0.033}$	$-0.09^{+0.44}_{-0.40}$	$0.00^{+0.46}_{-0.00}$
17	0.00047	$1.343^{+0.039}_{-0.039}$	$1.361^{+0.045}_{-0.033}$	$0.18^{+0.17}_{-0.11}$	$0.31^{+0.12}_{-0.14}$
17	0.00058	$1.217^{+0.057}_{-0.045}$	$1.271^{+0.039}_{-0.027}$	$-0.20^{+0.22}_{-0.20}$	$0.00^{+0.15}_{-0.00}$
17	0.00076	$1.175^{+0.033}_{-0.045}$	$1.199^{+0.033}_{-0.027}$	$-0.09^{+0.29}_{-0.35}$	$0.00^{+0.30}_{-0.00}$
24	0.00067	$1.373^{+0.033}_{-0.027}$	$1.385^{+0.033}_{-0.027}$	$0.21^{+0.13}_{-0.11}$	$0.29^{+0.12}_{-0.10}$
24	0.00082	$1.277^{+0.033}_{-0.027}$	$1.289^{+0.027}_{-0.027}$	$0.06^{+0.16}_{-0.13}$	$0.14^{+0.09}_{-0.12}$
24	0.00108	$1.193^{+0.033}_{-0.027}$	$1.205^{+0.033}_{-0.021}$	$0.09^{+0.28}_{-0.22}$	$0.19^{+0.19}_{-0.17}$
32	0.00089	$1.355^{+0.027}_{-0.027}$	$1.361^{+0.033}_{-0.021}$	$0.06^{+0.11}_{-0.11}$	$0.14^{+0.08}_{-0.11}$
32	0.00109	$1.271^{+0.027}_{-0.021}$	$1.283^{+0.027}_{-0.021}$	$0.13^{+0.16}_{-0.11}$	$0.22^{+0.12}_{-0.12}$
32	0.00143	$1.193^{+0.027}_{-0.027}$	$1.205^{+0.021}_{-0.021}$	$-0.02^{+0.23}_{-0.20}$	$0.00^{+0.23}_{+0.00}$
45	0.00125	$1.319^{+0.027}_{-0.027}$	$1.325^{+0.027}_{-0.021}$	$0.12^{+0.13}_{-0.10}$	$0.19^{+0.12}_{-0.09}$
45	0.00153	$1.259^{+0.027}_{-0.027}$	$1.271^{+0.027}_{-0.021}$	$0.06^{+0.14}_{-0.16}$	$0.09^{+0.11}_{-0.09}$
45	0.00202	$1.163^{+0.027}_{-0.021}$	$1.169^{+0.027}_{-0.021}$	$0.30^{+0.20}_{-0.23}$	$0.35^{+0.17}_{-0.21}$
60	0.00167	$1.319^{+0.033}_{-0.021}$	$1.331^{+0.027}_{-0.027}$	$0.12^{+0.14}_{-0.11}$	$0.19^{+0.12}_{-0.11}$
60	0.00204	$1.235^{+0.027}_{-0.021}$	$1.241^{+0.027}_{-0.021}$	$0.22^{+0.16}_{-0.17}$	$0.25^{+0.16}_{-0.14}$
60	0.00269	$1.133^{+0.027}_{-0.021}$	$1.145^{+0.027}_{-0.015}$	$0.04^{+0.25}_{-0.23}$	$0.09^{+0.21}_{-0.09}$
80	0.00222	$1.235^{+0.033}_{-0.027}$	$1.247^{+0.027}_{-0.027}$	$0.15^{+0.13}_{-0.14}$	$0.17^{+0.11}_{-0.11}$
80	0.00272	$1.223^{+0.033}_{-0.021}$	$1.229^{+0.033}_{-0.021}$	$0.45^{+0.14}_{-0.20}$	$0.44^{+0.19}_{-0.16}$
80	0.00359	$1.097^{+0.027}_{-0.021}$	$1.103^{+0.027}_{-0.015}$	$0.18^{+0.25}_{-0.23}$	$0.23^{+0.20}_{-0.18}$
110	0.00306	$1.187^{+0.033}_{-0.033}$	$1.199^{+0.033}_{-0.027}$	$0.12^{+0.16}_{-0.17}$	$0.16^{+0.12}_{-0.14}$
110	0.00374	$1.157^{+0.033}_{-0.033}$	$1.163^{+0.033}_{-0.027}$	$0.21^{+0.20}_{-0.22}$	$0.20^{+0.20}_{-0.14}$
110	0.00493	$1.037^{+0.027}_{-0.021}$	$1.049^{+0.027}_{-0.015}$	$-0.12^{+0.31}_{-0.23}$	$0.00^{+0.25}_{+0.00}$

combined statistical and uncorrelated systematic uncertainties. This procedure, and the use of ZEUS97 data, yielded a total of 104 reduced cross sections.

The procedure to extract F_L, F_2 and R is explained in the previous ZEUS publication [14]. Free parameters were introduced in the fits for each of the data sets to allow the normalization factors to vary according to Gaussian distributions with standard deviations given by the uncertainties quoted above for the HER, MER and LER data sets, respectively. The uncertainties for the central-vertex sample were used for $Q^2 \geq 17$ GeV^2, where these data dominated the combinations. The uncertainties for the shifted-vertex sample were used at lower Q^2, where they are more precise. The normalization of the ZEUS97 data was kept fixed in the fit. The resulting values of F_2 and F_L therefore have an additional uncertainty resulting from the normalization uncertainty of this data set (2%).

Additional nuisance parameters were introduced in the fits to account for the correlated systematic uncertainties.

All systematic uncertainties of the ZEUS97 data set were treated as uncorrelated with those of the HER, MER and LER samples. A global fit was performed to extract F_L and F_2 values from the reduced cross sections. The joint posterior probability distribution for all parameters was

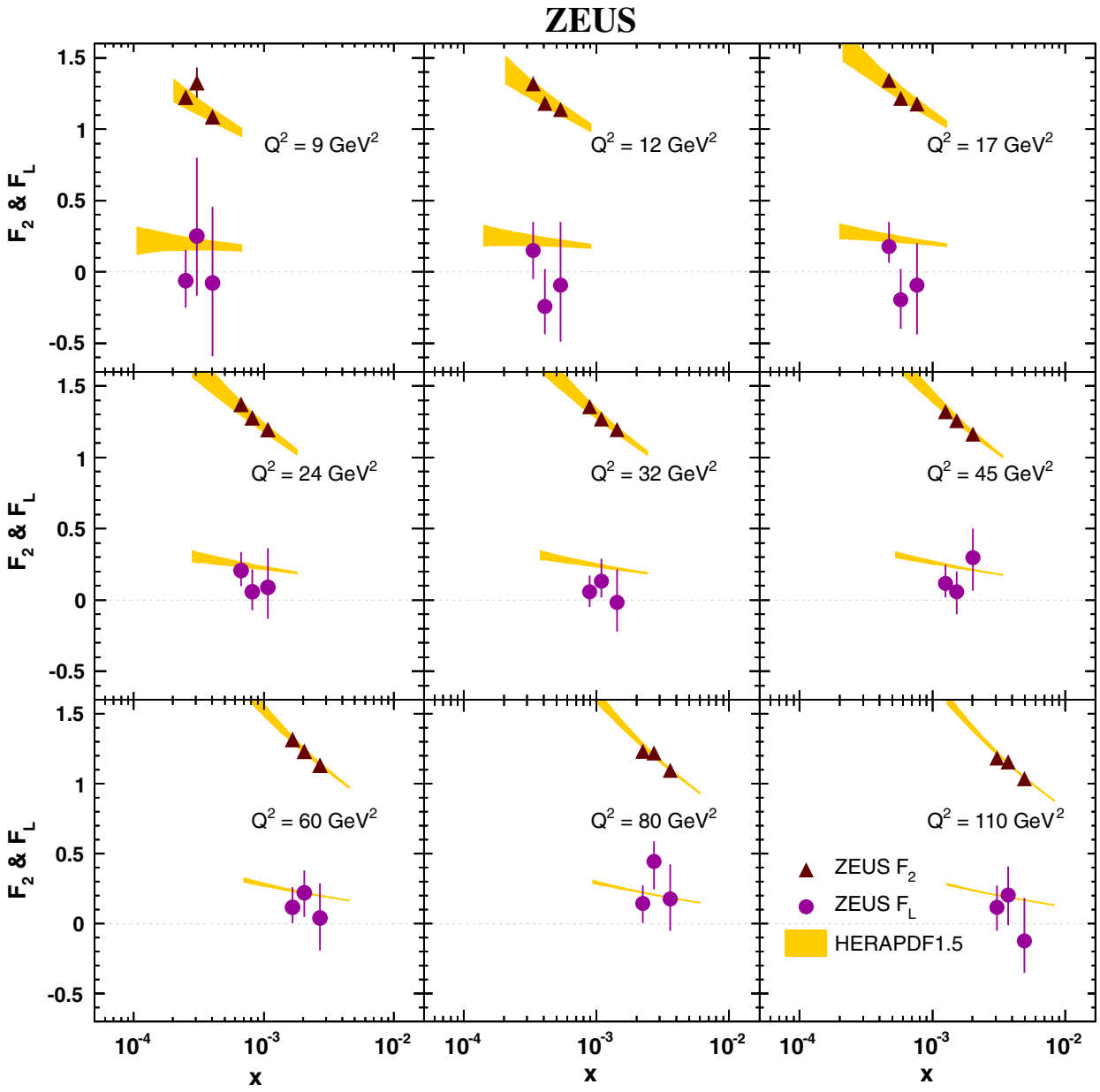

FIG. 8 (color online). F_L and F_2 values as a function of x for nine values of Q^2, extracted from the unconstrained fit (see Sec. IX B). The error bars on the data represent the combined statistical and systematic uncertainties. The error bars on F_2 are typically smaller than the symbols. NNLO QCD predictions from HERAPDF1.5 are also shown. The bands indicate the uncertainty in the predictions.

TABLE IX. Extracted values of F_L and R at 9 Q^2 points. Values are quoted for the unconstrained and constrained fits. The quoted uncertainties cover both the statistical and systematic sources. The normalization uncertainty (see Sec. IX A) is not included. For the constrained fits with mode at $F_L = 0$, the upper uncertainties correspond to 68% probability limits.

Q^2 (GeV^2)	$F_L(Q^2)$ (unconstrained fit)	$F_L(Q^2)$ (constrained fit)	$R(Q^2)$ (unconstrained fit)	$R(Q^2)$ (constrained fit)
9	$-0.04^{+0.19}_{-0.17}$	$0.00^{+0.14}_{-0.00}$	$0.01^{+0.17}_{-0.13}$	$0.05^{+0.17}_{-0.05}$
12	$-0.00^{+0.18}_{-0.16}$	$0.00^{+0.14}_{-0.00}$	$0.01^{+0.17}_{-0.12}$	$0.05^{+0.15}_{-0.05}$
17	$0.08^{+0.13}_{-0.10}$	$0.13^{+0.09}_{-0.10}$	$0.09^{+0.11}_{-0.10}$	$0.14^{+0.08}_{-0.11}$
24	$0.16^{+0.10}_{-0.12}$	$0.18^{+0.11}_{-0.08}$	$0.14^{+0.11}_{-0.07}$	$0.17^{+0.10}_{-0.08}$
32	$0.08^{+0.09}_{-0.09}$	$0.10^{+0.08}_{-0.08}$	$0.08^{+0.08}_{-0.07}$	$0.09^{+0.09}_{-0.05}$
45	$0.12^{+0.11}_{-0.09}$	$0.14^{+0.10}_{-0.08}$	$0.10^{+0.10}_{-0.06}$	$0.12^{+0.09}_{-0.08}$
60	$0.14^{+0.13}_{-0.09}$	$0.18^{+0.09}_{-0.10}$	$0.14^{+0.10}_{-0.09}$	$0.16^{+0.10}_{-0.09}$
80	$0.22^{+0.13}_{-0.11}$	$0.24^{+0.11}_{-0.10}$	$0.25^{+0.12}_{-0.12}$	$0.25^{+0.14}_{-0.11}$
110	$0.09^{+0.15}_{-0.10}$	$0.10^{+0.13}_{-0.08}$	$0.10^{+0.16}_{-0.10}$	$0.12^{+0.13}_{-0.09}$

then extracted under different sets of conditions as described below.

B. Fit results

Constrained and unconstrained parameter fits were performed to extract $F_2(x, Q^2)$ and $F_L(x, Q^2)$. Flat priors were used for the physics parameters within the range allowed. For the constrained fits, $0.8 < F_2 < 2$ and $0 \leq F_L \leq F_2$ were required. Example Rosenbluth plots [52] showing the linear fit to the reduced cross sections together with a 68% uncertainty band are shown in Fig. 7 for the nine lowest x points for each Q^2 bin for the unconstrained fits. The resulting F_2 and F_L values for all (x, Q^2) bins are given in Table VIII. The results given are for the parameter value at the mode of the marginalized probability distribution [51]. For each parameter, the narrowest 68% probability interval around the marginalized mode is taken as an uncertainty. These ranges contain the full experimental uncertainty. Relative uncertainties as small as 2% were achieved for F_2 and (absolute) uncertainties for F_L were in the range 0.1–0.2. The results for F_L found in this analysis are somewhat lower than those in the previous ZEUS analysis [14] in the region of kinematic overlap. The difference compared to the previous ZEUS analysis is primarily due to improvements in the treatment of the diffractive events in the MC simulation and of the electron validation at small scattering angles.

The results from the unconstrained fit are shown in Fig. 8 together with predictions based on the HERAPDF1.5 expectations. Reasonable agreement between extracted and predicted F_2 and F_L values is observed although with a tendency for the prediction to lie above the extracted F_L values.

Further fits to the data were performed to extract $F_L(Q^2)$, $R(Q^2)$, and a single overall value of R for the full data set. In each case, the same fitting procedure as described above was used, but with a reduced number of parameters.

To extract $F_L(Q^2)$, first $r(Q^2)$ was fitted, where $r = F_L/F_2$, taking a single value of r for all x points in the same Q^2 bin. The value of $F_L(Q^2)$ was then evaluated as $F_L(x_i, Q^2) = r(Q^2)F_2(x_i, Q^2)$, where for each Q^2 point, x_i was chosen such that Q^2/x_i was constant, which for

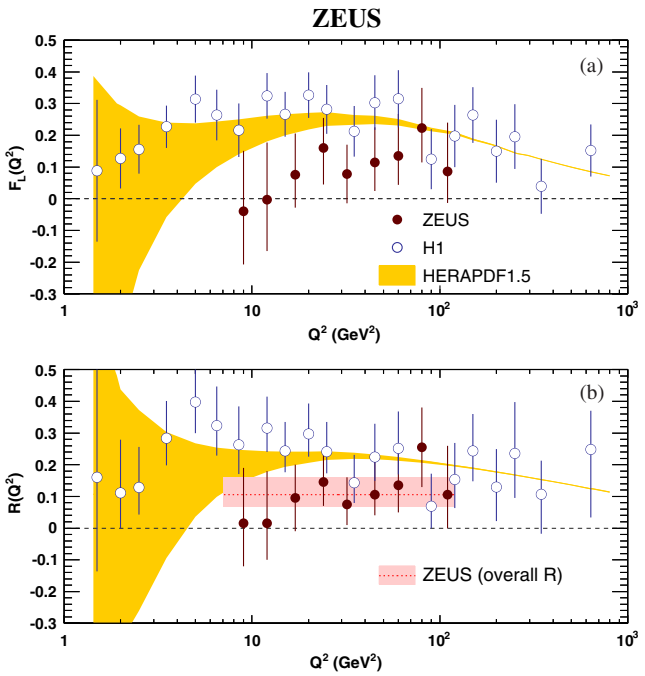

FIG. 9 (color online). Values of (a) F_L and (b) R as a function of Q^2. The ZEUS data, extracted from the unconstrained fit (see Sec. IX B) are shown as filled circles, with error bars representing the combined statistical and systematic uncertainties. The values of F_L at different Q^2 points are correlated, as well as the values of R. The shaded band labeled "ZEUS (overall R)" represents the 68% probability interval for the overall R. The H1 data are shown as open circles with error bars representing the total uncertainties. The ZEUS and H1 points are measured at somewhat different x values. NNLO QCD predictions from HERAPDF1.5 are also shown. The bands indicate the uncertainty in the predictions.

$\sqrt{s} = 225$ GeV corresponds to $y = 0.71$. Both constrained and unconstrained fits were made. For the constrained $R(Q^2)$ and overall R fits it was required that $R(Q^2) \geq 0$ and $R \geq 0$. The results for $F_L(Q^2)$ and $R(Q^2)$ are given in Table IX. The overall value of R from both the unconstrained and constrained fits is $R = 0.105^{+0.055}_{-0.037}$. In the previous ZEUS publication, a value of $R = 0.18^{+0.07}_{-0.05}$ was found. The difference is due to the extended kinematic range used here (the R values tend to be lower at lower Q^2) and the improved analysis. Figures 9(a) and 9(b) show a comparison of $F_L(Q^2)$ and $R(Q^2)$ with the H1 data [17] and the NNLO QCD predictions based on the HERAPDF1.5. The H1 measurements generally lie above the ZEUS results. The differences were examined: taking into account the correlations between the ZEUS data points and neglecting the correlations between the H1 data points a χ^2 of 12.2 is obtained for 8 degrees of freedom. The predictions based on HERAPDF1.5 are in reasonable agreement with both data sets.

X. SUMMARY

The reduced cross sections $\tilde{\sigma}(x, Q^2)$ for e^+p neutral current deep inelastic scattering have been measured with the ZEUS detector at HERA, using data collected at $\sqrt{s} = 318$, 251 and 225 GeV, in the kinematic region $0.13 \leq y \leq 0.75$ and $5 \leq Q^2 \leq 110$ GeV^2. The extension of the kinematic range in comparison to the previous ZEUS publication [14] was made possible with the use of shifted-vertex data. The new results supersede those in the previous publication. The reduced cross sections were used together with those from previous ZEUS data collected at $\sqrt{s} =$ 300 GeV to extract the proton structure functions F_2 and F_L for 27 values of x and Q^2. Relative uncertainties as small as 2% were achieved for F_2 and (absolute) uncertainties for F_L were in the range 0.1–0.2. In addition, F_L and the ratio, $R = F_2/(F_2 - F_L)$, have also been extracted as a function of Q^2 together with an overall value of $R = 0.105^{+0.055}_{-0.037}$. The F_L measurements reported here are lower than but compatible with those in the previous ZEUS and H1 publications and in reasonable agreement with theoretical predictions for F_L.

ACKNOWLEDGMENTS

We appreciate the contributions to the construction, maintenance and operation of the ZEUS detector made by many people who are not listed as authors. The HERA machine group and the DESY computing staff are especially acknowledged for their success in providing excellent operation of the collider and the data-analysis environment. We thank the DESY directorate for their strong support and encouragement. We thank H. Spiesberger for useful discussions concerning electroweak corrections. The following were supported by the Italian National Institute for Nuclear Physics (INFN): INFN Bologna, Bologna, Italy; University and INFN Bologna, Bologna, Italy; Calabria University, Physics Department and INFN, Cosenza, Italy; Dipartimento di Fisica dell' Università and INFN, Padova, Italy; Dipartimento di Fisica, Università "La Sapienza" and INFN, Rome, Italy; Università di Torino and INFN, Torino, Italy; and Università del Piemonte Orientale, Novara, and INFN, Torino, Italy. Physikalisches Institut der Universität Bonn, Bonn, Germany was supported by the German Federal Ministry for Education and Research (BMBF), under Contract No. 05 H09PDF. National Centre for Particle Physics, Universiti Malaya, 50603 Kuala Lumpur, Malaysia, was supported by HIR Grant No. UM.C/625/1/HIR/149 and UMRG Grants No. RU006-2013, No. RP012A-13AFR, and No. RP012B-13AFR from Universiti Malaya, and ERGS Grant No. ER004-2012A from the Ministry of Education, Malaysia. The Henryk Niewodniczanski Institute of Nuclear Physics, Polish Academy of Sciences, Krakow, Poland, and AGH-University of Science and Technology, Faculty of Physics and Applied Computer Science, Krakow, Poland, were supported by the National Science Centre under Contract No. DEC-2012/06/M/ST2/00428. The following were supported by the Science and Technology Facilities Council, UK: School of Physics and Astronomy, University of Glasgow, Glasgow, United Kingdom; Department of Physics, University of Oxford, Oxford, United Kingdom; and Physics and Astronomy Department, University College London, London, United Kingdom. Hamburg University, Institute of Experimental Physics, Hamburg, Germany was supported by the German Federal Ministry for Education and Research (BMBF), under Contract No. 05h09GUF, and the SFB 676 of the Deutsche Forschungsgemeinschaft (DFG). The following were supported by the Japanese Ministry of Education, Culture, Sports, Science and Technology (MEXT) and its grants for Scientific Research: Institute of Particle and Nuclear Studies, KEK, Tsukuba, Japan; Meiji Gakuin University, Faculty of General Education, Yokohama, Japan; Polytechnic University, Tokyo, Japan; and Department of Physics, Tokyo Institute of Technology, Tokyo, Japan. The following were supported by the Natural Sciences and Engineering Research Council of Canada (NSERC): Department of Physics, McGill University, Montréal, Quebec, Canada H3A 2T8; Department of Physics, University of Toronto, Toronto, Ontario, Canada M5S 1A7; and Department of Physics, York University, Ontario, Canada M3J 1P3. Lomonosov Moscow State University, Skobeltsyn Institute of Nuclear Physics, Moscow, Russia was supported by RF Presidential Grant No. 3042.2014.2 for the Leading Scientific Schools and by the Russian Ministry of Education and Science through its grant for Scientific Research on High Energy Physics. Raymond and Beverly Sackler Faculty of Exact Sciences, School of Physics, Tel Aviv University, Tel Aviv, Israel was

supported by the Israel Science Foundation. R. Aggarwal and P. Kaur were also funded by Max Planck Institute for Physics, Munich, Germany. I. Singh was also funded by Max Planck Institute for Physics, Munich, Germany, now at Sri Guru Granth Sahib World University, Fatehgarh Sahib. W. Słomiński was partially supported by the Polish National Science Centre Projects No. DEC-2011/01/B/ST2/03643 and DEC-2011/03/B/ST2/00220. V. Myronenko, O. Turkot, and K. Wichmann were supported by the Alexander von Humboldt Foundation. V. Aushev, Y. Aushev, V. Bokhonov, and N. Zhmak were supported by DESY, Germany. M. Wing was also supported by DESY.

[1] F. D. Aaron *et al.* (H1 and ZEUS Collaborations), J. High Energy Phys. 01 (2010) 109.
[2] Yu. L. Dokshitzer, Sov. Phys. JETP **46**, 641 (1977); V. N. Gribov and L. N. Lipatov, Sov. J. Nucl. Phys. **15**, 438 (1972); **15**, 675 (1972); G. Altarelli and G. Parisi, Nucl. Phys. **B126**, 298 (1977).
[3] H. L. Lai, M. Guzzi, J. Huston, Z. Li, P. M. Nadolsky, J. Pumplin, and C.-P. Yuan, Phys. Rev. D **82**, 074024 (2010).
[4] A. D. Martin, W. J. Stirling, R. S. Thorne, and G. Watt, Eur. Phys. J. C **63**, 189 (2009).
[5] M. Glück, P. Jimenez-Delgado, and E. Reya, Eur. Phys. J. C **53**, 355 (2008).
[6] P. Jimenez-Delgado and E. Reya, Phys. Rev. D **79**, 074023 (2009).
[7] R. D. Ball *et al.*, Nucl. Phys. **B867**, 244 (2013).
[8] S. Forte, E. Laenen, P. Nason, and J. Rojo, Nucl. Phys. **B834**, 116 (2010).
[9] S. Alekhin, J. Blümlein, and S. Moch, Phys. Rev. D **89**, 054028 (2014).
[10] J. J. Aubert *et al.*, Phys. Lett. **121B**, 87 (1983).
[11] A. C. Benvenuti *et al.* (BCDMS Collaboration), Phys. Lett. B **223**, 485 (1989).
[12] L. W. Whitlow, S. Rock, A. Bodek, S. Dasu, and E. M. Riordan, Phys. Lett. B **250**, 193 (1990).
[13] M. Arneodo *et al.* (New Muon Collaboration), Nucl. Phys. **B483**, 3 (1997).
[14] S. Chekanov *et al.* (ZEUS Collaboration), Phys. Lett. B **682**, 8 (2009).
[15] F. D. Aaron *et al.* (H1 Collaboration), Phys. Lett. B **665**, 139 (2008).
[16] F. D. Aaron *et al.* (H1 Collaboration), Eur. Phys. J. C **71**, 1579 (2011).
[17] F. D. Aaron *et al.* (H1 Collaboration), Eur. Phys. J. C **74**, 2814 (2014).
[18] F. D. Aaron *et al.* (H1 Collaboration), Eur. Phys. J. C **71**, 1836 (2011).
[19] S. Chekanov *et al.* (ZEUS Collaboration), Eur. Phys. J. C **21**, 443 (2001).
[20] ZEUS Collaboration, The ZEUS Detector, Status Report, DESY, 1993 edited by U. Holm (unpublished), available at http://www-zeus.desy.de/bluebook/bluebook.html.
[21] N. Harnew, G. P. Heath, M. D. Jeffs, J. Nash, G. L. Salmon, P. D. Shield, D. J. White, and F. F. Wilson, Nucl. Instrum. Methods Phys. Res., Sect. A **279**, 290 (1989); B. Foster *et al.*, Nucl. Phys. B, Proc. Suppl. **32**, 181 (1993); Nucl. Instrum. Methods Phys. Res., Sect. A **338**, 254 (1994).
[22] A. Polini *et al.*, Nucl. Instrum. Methods Phys. Res., Sect. A **581**, 656 (2007).
[23] M. Derrick, D. Gacek, N. Hill, B. Musgrave, R. Noland, E. Petereit, J. Repond, R. Stanek, and K. Sugano, Nucl. Instrum. Methods Phys. Res., Sect. A **309**, 77 (1991); A. Andresen *et al.*, Nucl. Instrum. Methods Phys. Res., Sect. A **309**, 101 (1991); A. Caldwell *et al.*, Nucl. Instrum. Methods Phys. Res., Sect. A **321**, 356 (1992); A. Bernstein *et al.*, Nucl. Instrum. Methods Phys. Res., Sect. A **336**, 23 (1993).
[24] A. Dwurazny, W. Krupinski, G. Barbagli, P. G. Pelfer, D. G. Cassel, R. Klanner, U. Kötz, W. Koch, J. Tengeler, and N. Wainer, Nucl. Instrum. Methods Phys. Res., Sect. A **277**, 176 (1989).
[25] A. Bamberger *et al.* (ZEUS Collaboration), Nucl. Instrum. Methods Phys. Res., Sect. A **401**, 63 (1997).
[26] T. Gosau, Ph.D. thesis, FB Physik, University Hamburg, Germany [Report No. DESY-THESIS-2007-028, 2007; M. Schröder, Diploma thesis, FB Physik, University Hamburg, Germany [Report No. DESY-THESIS-2008-039, 2008].
[27] J. Andruszków *et al.*, Report No. DESY-92-066, DESY, 1992; M. Derrick *et al.* (ZEUS Collaboration), Z. Phys. C **63**, 391 (1994); J. Andruszków *et al.*, Acta Phys. Pol. B **32**, 2025 (2001).
[28] M. Helbich, Y. Ning, S. Paganis, Z. Ren, W. B. Schmidke, F. Sciulli, U. Schneekloth, C. Büttner, A. Caldwell, and J. Sutiak, Nucl. Instrum. Methods Phys. Res., Sect. A **565**, 572 (2006).
[29] L. Adamczyk *et al.* (ZEUS Collaboration), Nucl. Instrum. Methods Phys. Res., Sect. A **744**, 80 (2014).
[30] H. Spiesberger, *HERACLES and DJANGOH: Event Generation for ep Interactions at HERA Including Radiative Processes* (DESY, Hamburg, Germany, 1998), available at http://wwwthep.physik.uni-mainz.de/~hspiesb/djangoh/djangoh.html.
[31] H. Spiesberger, An event generator for ep interactions at HERA including radiative processes, Version 4.6, DESY, Hamburg, Germany, 1996, available at http://www.desy.de/~hspiesb/heracles.html.
[32] G. Ingelman, A. Edin, and J. Rathsman, Comput. Phys. Commun. **101**, 108 (1997).
[33] T. Sjöstrand, Comput. Phys. Commun. **39**, 347 (1986).
[34] H. L. Lai, J. Huston, S. Kuhlmann, J. Morfin, F. Olness, J. F. Owens, J. Pumplin, and W. K. Tung (CTEQ Collaboration), Eur. Phys. J. C **12**, 375 (2000).
[35] T. Sjöstrand *et al.*, PYTHIA 6.2: Physics and manual, 2001, available at http://home.thep.lu.se/~torbjorn/pythiaaux/past.html; Comput. Phys. Commun. **135**, 238 (2001).

[36] M. Glück, E. Reya, and A. Vogt, Z. Phys. C **53**, 127 (1992).
[37] T. Abe, Comput. Phys. Commun. **136**, 126 (2001).
[38] T. Sjöstrand, Comput. Phys. Commun. **82**, 74 (1994).
[39] R. Brun *et al.*, Report No. CERN-DD/EE/84-1, 1987 (unpublished).
[40] A. Arbuzov, D. Bardin, J. Blümlein, L. Kalinovskaya, and T. Riemann, Comput. Phys. Commun. **94**, 128 (1996).
[41] P. Kaur, Ph.D. thesis, Chandigarh University, India, 2012 (unpublished)
[42] K. C. Höger, in *Proceedings of the Workshop on Physics at HERA*, edited by W. Buchmüller and G. Ingelman (DESY, Hamburg, Germany, 1992), Vol. 1, p. 43.
[43] R. Sinkus and T. Voss, Nucl. Instrum. Methods Phys. Res., Sect. A **391**, 360 (1997); H. Abramowicz, A. Caldwell, and R. Sinkus, Nucl. Instrum. Methods Phys. Res., Sect. A **365**, 508 (1995).
[44] J. Breitweg *et al.* (ZEUS Collaboration), Eur. Phys. J. C **1**, 109 (1998).
[45] W. H. Smith *et al.*, Nucl. Instrum. Methods Phys. Res., Sect. A **355**, 278 (1995).
[46] W. H. Smith, K. Tokushuku, and L. W. Wiggers, in *Proceedings of Computing in High-Energy Physics (CHEP), Annecy, France*, edited by C. Verkerk and W. Wojcik (CERN, Geneva, Switzerland, 1992), p. 222.
[47] S. Shimizu, Ph.D. thesis, University of Tokyo, Japan, 2009 [KEK-report 2009-1]
[48] F. Jacquet and A. Blondel, in *Proceedings of the Study for an ep Facility for Europe*, edited by U. Amaldi (DESY, Hamburg, Germany, 1979), p. 391.
[49] V. Radescu, arXiv:1308.0374.
[50] J. Schwartz, Ph.D. thesis, McGill University, Montreal, Quebec, 2011 (unpublished).
[51] A. Caldwell, D. Kollár, and K. Kröninger, Comput. Phys. Commun. **180**, 2197 (2009).
[52] M. N. Rosenbluth, Phys. Rev. **79**, 615 (1950).